Water Resources Research

RESEARCH ARTICLE
10.1029/2023WR034978

Experimental Study on Influence of Different Patterns of an Emergent Vegetation Patch on the Flow Field and Scour/Deposition Processes in the Wake Region

Oral Yagci[1], V. S. Özgur Kirca[2], Vasileios Kitsikoudis[3], Catherine A. M. E. Wilson[4], M. Furkan Celik[5], and Caner Sertkan[2]

[1]Civil Engineering Department, Engineering Faculty, Aydin Adnan Menderes University, Aydin, Turkey, [2]Civil Engineering Department, Istanbul Technical University, Istanbul, Turkey, [3]Department of Water Engineering and Management, Faculty of Engineering Technology, University of Twente, Enschede, The Netherlands, [4]Hydro-Environmental Research Center, School of Engineering, Cardiff University, Cardiff, UK, [5]Geomatics Engineering Department, Civil Engineering Faculty, Istanbul Technical University, Istanbul, Turkey

Key Points:

- Experiments were conducted to see the impact of different patterns of an emergent vegetation patch on flow field and scour in rivers
- Streamlined bodies are hydrodynamically favorable bodies. Yet, tests showed that the elongation of patches increases scour and localization
- The steady-wake zone becomes shorter as the patch elongated, hence restricting the patch's expansion

Supporting Information:

Supporting Information may be found in the online version of this article.

Correspondence to:

O. Yagci,
oral.yagci@adu.edu.tr

Citation:

Yagci, O., Özgur Kirca, V. S., Kitsikoudis, V., Wilson, C. A. M. E., Furkan Celik, M., & Sertkan, C. (2024). Experimental study on influence of different patterns of an emergent vegetation patch on the flow field and scour/deposition processes in the wake region. *Water Resources Research*, *60*, e2023WR034978. https://doi.org/10.1029/2023WR034978

Received 13 APR 2023
Accepted 14 NOV 2023

Author Contributions:

Conceptualization: Oral Yagci
Data curation: V. S. Özgur Kirca, M. Furkan Celik
Formal analysis: Vasileios Kitsikoudis, Catherine A. M. E. Wilson, M. Furkan Celik, Caner Sertkan
Investigation: M. Furkan Celik, Caner Sertkan
Methodology: Oral Yagci, V. S. Özgur Kirca

Abstract Flume experiments were conducted to comprehend the impact of different patterns of an emergent vegetation patch on the flow field and the scour process in natural rivers. Velocity measurements, flow visualization, and scour tests were undertaken around different vegetation patch patterns, which were simulated inspired by the expansion process of a typical instream vegetation. The patch expansion process was idealized with an initially circular patch of rigid emergent stems becoming elongated due to positive and negative feedbacks. The expansion of the vegetation patch was considered to occur in three stages, in which the density of the patch from the previous stage was increased while the patch was also elongated by connecting at its downstream side with another sparser vegetation patch. These stages were replicated succesively by increasing the density and elongating the patch. In this way, two processes (i.e., elongation and decrease in permeability), which usually have hydrodynamically opposite effects on flow fields, were simulated at the same obstruction. Despite generally elongated obstacles being streamlined bodies, the morphometric analysis obtained by laser scanner revealed that streamlined elongation of permeable patches amplifies global scour and enhances localization of the local scour hole. This situation implies that as the patch expands, in the wake region, the steady-wake region becomes shorter, turbulence diminishes, lateral shear stress enhances, and deposition cannot occur far from the patch. Consequently, as the patch expands, the hydrodynamic consequences may restrict further patch expansion after a certain length/density.

Plain Language Summary What effect does enlarging a single patch have on the local flow field and scour pattern? This research question was examined experimentally. Despite the fact that streamlined patches are hydrodynamically favorable formations, morphometric scour measurements show that the streamlined extension of permeable patches increases global scour and promotes local scour hole localization. As the patch develops, the steady-wake zone of low velocity and suppressed turbulence that favors sediment entrapment decreases restricting its expansion.

1. Introduction

Landform evolution of river systems is governed mainly by the interaction of flowing water with sediment and vegetation (Gurnell, 2014; Larsen, 2019). The vegetation drag leads to complex flow patterns both at the patch (Luhar & Nepf, 2013; Schnauder & Moggridge, 2009) and reach scales (Yagci and Strom, 2022; Yamasaki et al., 2019) with direct implications to sediment entrainment and deposition (Follett & Nepf, 2012; Ortiz et al., 2013). The mosaic of bed material in vegetated rivers is rich in organic matter and nutrient content (Jones et al., 2012), and its redistribution across the river system leads to biogeomorphic mechanisms (Camporeale et al., 2013; Solari et al., 2016) that may promote or impede the establishment and proliferation of new vegetation.

The accurate foreseen of the evolution of vegetation coverage is also needed for the development of sustainable river management/restoration strategies (Palmer et al., 2005). The increase of vegetation biomass was traditionally regarded as a source of increase in roughness, and assumed that it reduces the conveyance capacity of the river (Bal et al., 2011; Yuksel, 2018). Yet, the study by Cornacchia et al. (2022) pointed out evidences that submerged aquatic plants maintain required water levels for the aquatic ecological system at low discharges.

Resources: Vasileios Kitsikoudis, Catherine A. M. E. Wilson, M. Furkan Celik, Caner Sertkan
Supervision: Oral Yagci, V. S. Özgur Kirca
Visualization: Oral Yagci, V. S. Özgur Kirca
Writing – original draft: Oral Yagci, V. S. Özgur Kirca, Vasileios Kitsikoudis

Likewise, the reach-scale experiments conducted by Yagci and Strom (2022) revealed that instream vegetation acts like a natural weir, produces a backwater effect and augments the residence time. Hence, the presence of vegetation can be sought as it constitutes an integral component of sustainable river and estuarine ecosystems. The presence of vegetation in river systems and shoreline areas is widely acknowledged as a substantial and ever-changing element of the ecosystem (Heidelman & Vural, 2023; Turker et al., 2019). The experiment conducted by Holzenthal et al. (2022) demonstrated the interplay among waves, sediment, and flexible vegetation. A shoreward depositional mound was observed even when the plant blades were flexed to approximately one-third or less of their maximum height. This flexibility occurred as a result of a decrease in velocity caused by the presence of the plant obstruction. The findings of this study are of considerable importance, as they illustrate the substantial impact of vegetation on the formation of sediment bedforms, not only within river systems but also within coastal regions.

These self-organized instream plant communities and islands provide flow variability in the active channel (Heidari et al., 2021; Schwarz et al., 2018), enhance the ecosystem resilience under repeated cycle of discharge fluctuations (Cornacchia et al., 2022), enrich the riverine biodiversity (Stein et al., 2014; Wharton et al., 2006). Gurnell (2014) highlighted the role of vegetation as an ecosystem engineer, and recognized that the complex intertwined relationship between flow, sediment and vegetation that affects the biogeomorphic processes at the patch scale, can have a distinct large-scale geomorphologic impact. The interplay between biotic (vegetation patch and seedlings) and abiotic (water and sediment) factors leads to an expansion of vegetation patches in the streamwise direction (Jones et al., 2012; Sand-Jensen & Pedersen, 2008; Yamasaki et al., 2019), with the driving mechanism for this evolution being a combination of negative and positive feedbacks (Bouma et al., 2009).

The current flood control measures increasingly focus on enlargement of floodplains to mitigate the devastation caused by high- intensity-low-frequency floods in which prone to be more frequently observed due to climate change (Bardossy & Caspary, 1990). In this context, woody vegetation such as *Ulmus* species (Vreugdenhil et al., 2006; Ward et al., 2002), and tree-like species like *Salix*, *Populus* (Wilson, Yagci, Rauch, & Olsen, 2006), and *Alnus* (Vreugdenhil et al., 2006), that form on the river active zones and on midchannel islands, would be subjected to flooding more often than it used to be. A more comprehensive understanding of the intricate reciprocal relationship between flow, vegetation, and sediment is necessary in this case. The formation of process of instream patches was discussed in detail below.

1.1. Flow Kinematics Around an Isolated Patch

To estimate the anticipated elongation of a vegetation patch, the extent of the deposition zone in the wake of the patch is needed to be determined based on the induced hydrodynamic pattern. The velocity difference between the contracted flow at the sides of an isolated patch and the slow-moving fluid immediately downstream of the patch leads to the development of a shear layer at each side of the patch. These two shear layers grow linearly (Zong & Nepf, 2012) and eventually they meet along the patch centerline. The interaction of these two shear layers enhances turbulent mixing and may lead to the formation of a von Karman vortex street (Zong & Nepf, 2012), with some similarities to what is observed in the wake of a solid cylinder (Kitsikoudis et al., 2017), but with the notable difference that the von Karman vortex street is formed further downstream (Chen et al., 2012; Kitsikoudis et al., 2016). Huai et al. (2021) state that the streamwise momentum that passes through the permeable body limits the interaction between the two shear layers that form on both sides of the patch. This stops the von Karman vortex street from forming on the scale of the patch. The mean velocities and turbulence intensities from the rear edge of the patch until the point where the two shear layers meet remain relatively low, and they rise steeply afterward due to the intense turbulent mixing (Chen et al., 2012; Kitsikoudis et al., 2020). This area of low velocity and turbulence is known as the steady-wake region and its length indicates the potential area where suspended sediment can deposit (Chen et al., 2012; Ortiz et al., 2013). This length depends largely on the density of the patch and the flow that penetrates in the patch, that is, with sparse patches delaying the interaction of the shear layers and dense patches exhibiting a wake that resembles the wake of a solid cylinder (Chen et al., 2012; Lima et al., 2015; Zong & Nepf, 2012). In their study, Liu et al. (2021) conducted numerical simulations to examine the flow characteristics through a submerged patch. The velocities of the bleed flow, which refers to the flow that permeates through the body, were quantified by Liu et al. (2021) at the array's exit points. The data presented in their study demonstrated a logarithmic decrease in bleeding velocities as canopy density increased. Kingora and Sadat (2022) investigated the flow through a group of cylinders at the stem scale numerically. Their findings

demonstrated a monotonic decrease in drag force exerted on individual members as the solid fraction increased. Moreover, it was seen that when the solid fractions are low, the wakes generated behind stems located in the upstream part of the patch exhibit quasi-periodic characteristics, while the wakes formed behind stems in the downstream part demonstrate aperiodic behavior. At an intermediate solid fraction, the flow pattern in the wake behind each stem member remains steady. However, for members with a high solid fraction, the flow exhibits creeping behavior.

1.2. Formation/Expansion Stages of Vegetation Patches

In natural rivers, the entrainment of bedload overwhelmingly takes place during rising stage of high flows (Song & Graf, 1996). Yet, suspended sediment input exhibits a more complex character compared to bedload during the passage of infrequent flows. According to Klein (1984) a clockwise hysteresis occurs (where abscissa refers to water discharge, ordinate denotes sediment discharge) when sediment is derived from the bed and banks of the channel or areas neighboring to it, whereas an anti-clockwise hysteresis arises when the upper part of the slopes is the sediment source area. However, in spite of this complicated relationship between suspended sediment and discharge, it can be hypothesized that the suspended sediment concentration correlates well with the peak of the direct surface runoff in main channel. This situation is valid not only for the suspended sediment transport (Silva et al., 2023; Wang et al., 2021), but also the bedload (Wu et al., 2021), and pollutant transport (Stride et al., 2023) in natural vegetated rivers.

Particularly during the recession stage of a direct runoff hydrograph, the transportation ability of flow is less compared to that of the rising stage. The localized sediment mounds, which constitute a good basis for the sprout of vegetative fragments and propagules, forms during the falling stage of the direct runoff hydrograph on the river bed (Kuhnle, 1992; Reid et al., 1985) due to hysteresis in hydrograph (Kohandal-Gargari et al., 2021) as is picturized/referenced in Figure 1 and Table 1. Likewise, hydrochory (i.e., the process of propagule transport under the influence of direct runoff; Danvind & Nilsson, 1997), also affects the spatial expansion of instream plants in the channel.

Areas of low velocity and turbulence support the establishment of vegetation, while zones where the flow gets accelerated and turbulence increases lead to less favorable conditions (Jones et al., 2012; Schoelynck et al., 2012; Yager and Schmeeckle, 2013). Isolated instream plant elements sprout and grow during base flow, following the recession stage, if vegetative fragments are buried in the deposited sediment mounds (Gurnell et al., 2012). These sprouting and growing individual plant elements control coherent flow structures in their vicinity (Kitsikoudis et al., 2016) and provide suitable flow conditions (drop in velocity and shear stress) in their wake (Kitsikoudis et al., 2020) for the reproduction of other vegetation elements. The contraction-induced acceleration around the patch (Kitsikoudis et al., 2016) constitutes a negative feedback, which does not allow sediment to settle and inhibits the lateral expansion of the patch (Temmerman et al., 2007). Conversely, positive feedback, that is, the low velocity and suppressed turbulence within the wake region of the vegetation patch, promotes the deposition of the incoming suspended sediment and organic matter (Ortiz et al., 2013).

1.3. Scope of the Study

In vegetated rivers, the patch expansion is a gradually occurring continuous process. In this study, for the sake of simplicity, this expansion process was discretized and represented by three consecutive characteristic stages of the patches. Patches with different patterns and densities (Figure 1 and Table 1) were used during the experimentation. In this way, the influence of patch expansion on flow kinematics was investigated experimentally for these stages on rigid bed conditions with Eulerian (point measurements by ADV, i.e., acoustic Doppler velocimeter) and Lagrangian (flow visualization) measurements. This is followed by morphometric tests, which aim to observe the influence of the patch expansion on the scour.

Zong and Nepf (2012) showed that for a given permeable circular patch, the increased solid volume fraction, (i.e., decreased porosity) causes a decrease in the strength of the bleed flow, and the length of steady wake region. Decreased permeability also leads to an increase in the recovery distance of flow. On the other hand, as shown by Kitsikoudis et al. (2017), the elongation of an obstacle's cross-section leads to a reduction in the strength of the lee-wake vortices. This suggests that when the pile's cross-section is elongated, the body acquires a more hydrodynamic form. In other words, despite enhanced skin friction, the obstacle gains a favorable (i.e., less resistant

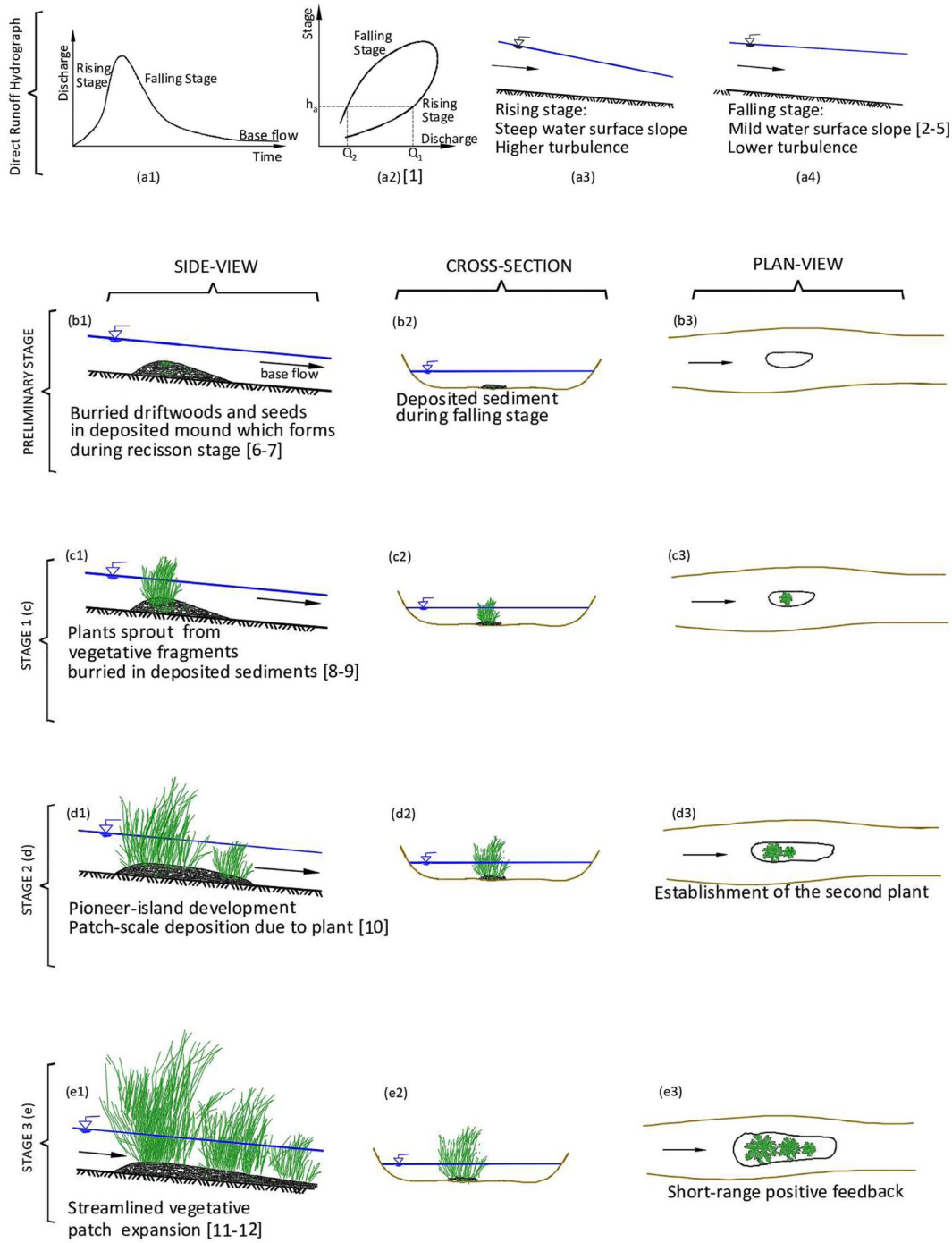

Figure 1. The consecutive stages of the expansion process of instream vegetation. The numbers in square brackets point out the reference studies (Table 1) which were used during the compilation of the figure.

against flow) hydrodynamic form with the elongation of the body exposed to flow. In their experiments, they have also witnessed that the recovery zone is shorter for a cylinder with an elongated cross-section. While the patch evolves to a more streamlined form, the patch expansion process contains two mutually exclusive hydrodynamic factors. These are:

1. Shortening of recovery zone due to an increase in the density of the patch.
2. Elongation of the recovery zone due to the streamlined shape of the body.

Table 1
Basic Findings in the Pertinent Literature Regarding the Successive Stages of Instream Patch Expansion Illustrated in Figure 1

Reference # in Figure 1	References	Remarks (quotations)	Relevance in Figure 1
[1]	Chow (1959)	"For a given stage, the discharge is higher on the rising limp of flood hydrograph."	Figure 1a2
[2]	Bayazit (2001)	"Water surface slope is steeper during rising stage"	Figures 1a2–1a3
[3]	Song and Graf (1996)	"During the passage of a hydrograph, the turbulence intensities and the Reynolds stress in the rising branch are larger than in the falling branch."	Figures 1a2–1a3
[4]	Reid et al. (1985)	"When flood's follow each other closely, the bed material is comparatively loose and offers less resistance to entrainment. In this case, substantial amounts of bedload are generated on the rising limb."	Figures 1a2–1a3
[5]	Kuhnle (1992)	"…significant differences in mean bed load transport rates were found at nearly all flow strengths. At higher flow strengths, mean bed load transport rates were greater during rising stages than during falling stages."	Figures 1a2–1a3
[6]	Gurnell and Petts (2002)	"The initial rise in water levels at the commencement of the high flow season can pick up and disperse numerous seeds and vegetative propagules"	Figures 1b1–1b3
[7]	Yagci and Strom (2022)	"During the recession stage, depending on the existing secondary flow pattern in the channel, which emerges as a response to the planform view and geometry of the channel, sediment begins to accumulate, particularly on the margins or in the middle of the channel"	Figures 1b1–1b3
[8]	Yagci and Strom (2022)	"…remarkable localized deposition zones were recorded within the wake region, at approximately 2–3 D distance to the downstream edge of the patch.""Vegetative fragments/propagules buried in these deposited sediments sprout, grow, and produce favorable flow conditions in their wake regions for the other plants."	Figures 1c1–1c3
[9]	Chen et al. (2012)	"The flow exiting the patch is laterally uniform and slower than the flow that passes around the patch. The streamwise velocity at the centerline remains at a constant value over the majority of the steady wake region."	Figures 1b1–1b3
[10]	Cornacchia et al. (2022)	"The steady wake represents a rather large, sheltered zone in the middle of a running-water environment, which plays a significant role in habitat creation, growth, and establishment of other organisms."	Figures 1d1–1d3
[11]	Schoelynck et al. (2012)	"It was proven that the conditions within the patches favored the survival and growth of transplants (i.e., short-range positive feedback), while the conditions just next to patches led to decreased survival and growth (i.e. long-range negative feedback)"	Figures 1e1–1e3
[12]	Gurnell et al. (2012)	"At the same time, certain aquatic and riparian plant species (including the dead wood they produce), are particularly important for initiating the trapping and stabilization of fluvially-transported sediments, constructing distinct pioneer landforms, and accelerating the development of larger landforms such as river banks, vegetated islands and floodplains"	Figures 1e1–1e3

Note. The expressions were directly quoted from the references to give the storyline of the examined process more accurately.

These two factors may affect the flow-patch interaction at different weights. In order to examine the role of the patch expansion process on flow and sedimentary processes, three patch cases were experimentally examined from a kinematic and morphologic perspective. Specifically, the experiments were designed to address the following research questions:

1. In the wake zone, how does the patch expansion process alter the mean flow and turbulence characteristics?
2. How does the patch expansion influence the flow recovery in the wake region?
3. How does the expansion process of the patch change the formation of vortices?
4. Under clear water circumstances, how does patch expansion affect the morphometric pattern of the scour/deposition zone?

As evident from the summary of the given above, the literature encompasses numerous studies that aim to identify the reciprocal interplay among flow, vegetation, and sediment at the patch scale. However, the existing literature lacks any studies that specifically investigate the relationship between a streamlined vegetation patch and its influence on flow patterns, as well as the subsequent effects on scour and deposition processes within river systems. Hence, the primary objective of this study was to experimentally examine the effects of different configurations of streamlined emergent vegetation patches on the flow field and the occurrence of local and global scour. The Methods section defines the conceptualizations utilized in representing streamlined vegetation

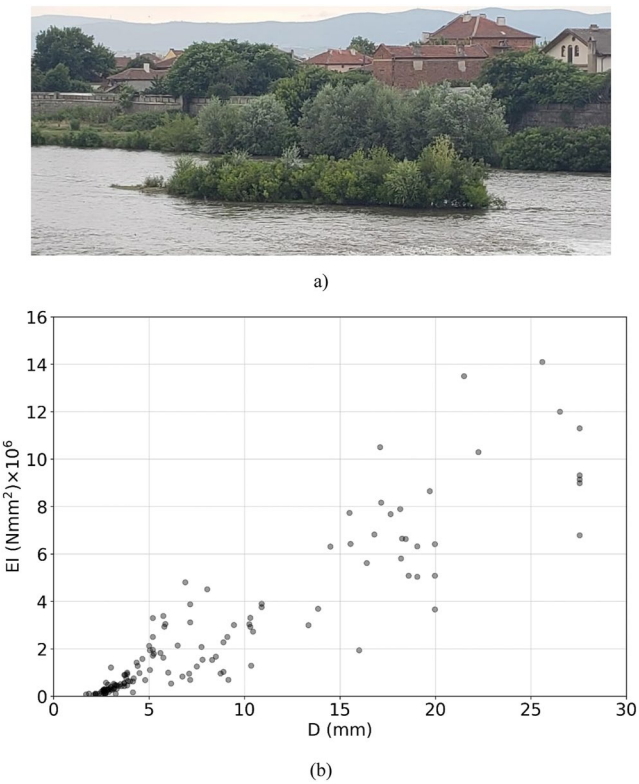

Figure 2. (a) A view of a midchannel island and the distribution of vegetative elements in Maritsa River, the flow direction is from right to left, (b) the variation of flexural rigidity of *Salix fragilis* (commonly known as crack willow) with respect to diameter.

patches during the experiments, based on the examination of pertinent literature and biomechanical measurements that we have made within the scope of this study. The key findings of this study are presented in the Results section, followed by the Discussion section, where an interpretation of the findings is presented within the context of river morphology, drawing upon existing literature. The major findings drawn from the experimental data are highlighted in the Conclusion section.

2. Methodology

2.1. Flume

The experiments were conducted at the Hydraulics Laboratory of Istanbul Technical University. The experimental facility comprised a recirculating flume, with a length of 26 m and a width of 0.98 m, with the flow being regulated by two pumps and a tailgate weir at the downstream end. The flume had a prismatic cross-section with a bed and sidewalls made of smooth concrete and Plexiglas, respectively. The bed of the flume was horizontal. At the inlet of the flume, the cross-section was filled with small tubes aligned with the flow direction to straighten the incoming flow and eliminate large swirls from the flow recirculation. The flow was kept steady with a water depth of 0.31 m for all experiments.

2.2. Characterization of Patch Expansion Process

For a vegetative patch, plant size distribution along the islands is quite typical. The height of the plant located at upstream is higher since it is established earlier compared to ones located at downstream (Gurnell & Petts, 2002) during the formation period. The plant first established on the riverbed creates favorable flow conditions in its wake region for the establishment of the new plants. Vegetation propagules are deposited and buried by sediments (Ward et al., 1999) in the wake region of this first established vegetation. As demonstrated previously based on riparian plant measurements (i.e., *Salix fragilis*, commonly known as crack willow) by Wilson, Yagci, Rauch, and Steosser (2006; Figure 4), with the increase of the isolated plant height, cumulative volume of the plants increases. Thus, it can be deduced that the vegetative elements located upstream have higher volume compared to one located at downstream. The view in Figure 2a confirms this assertion qualitatively as well. Furthermore, Wilson, Yagci, Rauch, and Steosser (2006) also found that the cumulative plant volume increases linearly with the basal diameter. Besides, the flexural rigidity measurements that we carried out in Cardiff University, Mechanical Engineering Laboratory, clearly revealed that flexural rigidity of *Salix fragilis* increases linearly (i.e., higher resistance by vegetation against bending) with respect to trunk/branch diameter (Figure 2b), which is relevant to vegetation age. In summary, it is plausible to expect that the vegetation elements located at the upstream part of the patch generate more hydraulic resistance against the flow compared to the ones located downstream, due to the fact that the pioneer plants located at the upstream part of an expanded patch have higher volume, basal diameter, and flexural rigidity.

Table 2
Characteristics of Vegetation Patches

Patch	D (cm)	Number of stems	d (cm)	α (m^{-1})	αD (−)	ϕ (−)
Dense	9	61	0.5	47.9	4.3	0.188
Medium	9	37	0.5	29.1	2.6	0.114
Sparse	9	19	0.5	14.9	1.3	0.059

The vegetation patches in this study were represented by circular arrays of emergent solid cylinders in a staggered arrangement. The circular arrays had a diameter, D, equal to 0.09 m, while all internal cylinders had a diameter, d, equal to 0.005 m. The internal cylinders were made of steel and were covered with a very thin layer of anti-rust paint. Three different arrays were assembled, with the number of internal cylinders being 61, 37, and 19 (Table 2), for a dense, medium, and sparse patch, respectively. The density of each patch is quantified by the frontal area per unit volume, $\alpha = nd$, and the solid volume fraction (SVF), $\phi = n\pi d^2/4$, where n is the number of cylinders per unit bed area. In other terms, the solid volume fraction is the ratio between the entire

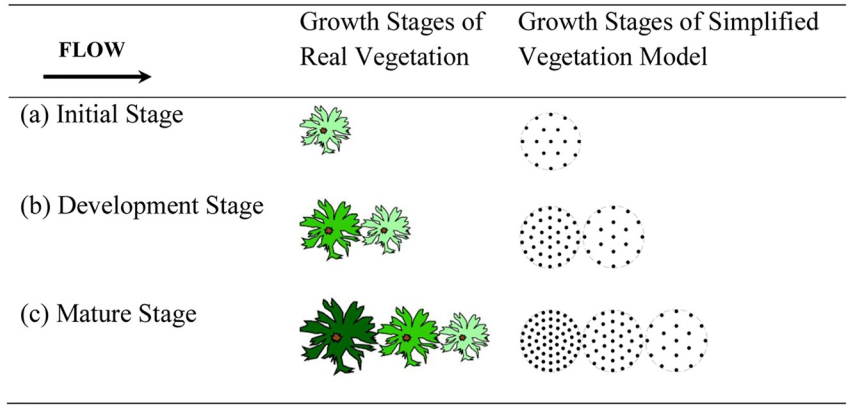

Figure 3. Planview sketches of the arrays of cylinders used in this study to simulate (a) initial, (b) development, and (c) mature stages. The diameter, D, of each array of cylinders is 9 cm and the diameter, d, of each cylinder is 0.5 cm.

area of all stems inside the colony area/to the colony area limited by circumambient diameter. These density characteristics are presented in Table 2, which classifies the three patches as dense, medium, and sparse, respectively, to facilitate their discussion in the paper.

As explained in the Introduction section, based on previous studies, a patch entraps suspended sediment and propagules in its wake, leading to establishment of new vegetation. It is assumed that once new vegetation stems are established and grown in the wake of the initial patch, the patch will become elongated in the streamwise direction, with the aboveground biomass being reduced in the streamwise direction. By aligning the vegetation patches in a row, the natural progression of this pattern is simulated in the experiments. Specifically, the following three setups are studied to express different growing stages of a vegetation patch: (a) flow through an isolated sparse patch: stage 1 (Figure 3a), (b) flow through a medium patch followed by a sparse patch: two patches, stage 2 (Figure 3b), and (c) flow through a dense patch followed by a medium and a sparse patch: stage 3 (Figure 3c). This idealized experimental setup simplifies what has been observed in natural rivers, where the width at the upstream side of the elongated patch is greater than the width at the downstream end (Sand-Jensen & Pedersen, 2008). The upstream side of the patch is bigger because the vegetative element placed most upstream developed first (Figure 1) and had more time to expand than the others. The medium and dense patches are also studied individually but solely as reference cases since flow around an isolated vegetation patch is well documented in the literature (Chen et al., 2012; Zong and Nepf, 2012). All vegetation patches studied herein were placed in the middle of the flume width and sufficiently downstream from the flume inlet where the flow is fully developed.

2.3. Flow Visualization, Velocity Measurements and Data Processing

Flow velocities were measured with a Nortek Vectrino Profiler with a down-looking probe at selected points along the centerline of the patch, and across the horizontal plane mid-depth, similar to Chen et al. (2012) and Zong & Nepf (2012). The measurements grid consisted of measurement points around and in the wake of the patches, with the measurement points being denser close to the patches to reproduce the expected steep velocity gradient around them (Figure 4). The Vectrino was mounted on a rolling platform above the flume that allowed its accurate relocation. The sampling frequency of the Vectrino was set to 100 Hz. The sampling duration at each measurement point was 100 s. To determine the required sampling duration to obtain unbiased turbulence statistics, preliminary experiments were conducted similar to Yagci and Kabdasli (2008). The obtained three-dimensional velocity components are denoted by u, v, and w for the longitudinal (x), transverse (y), and vertical (z) directions, respectively.

The water that was used for the flume experiments was extracted from a neighboring lake and had a relatively high concentration of suspended particles that provided seeding for the Vectrino measurements. The sampling volume was located 0.05 m below the probe of the Vectrino, which is the point that provides the most accurate measurements (Thomas et al., 2017). As a result, the signal-to-noise ratio and the correlation of the Vectrino measurements were sufficiently high to secure high-quality data. Nevertheless, high quality statistics of measurements

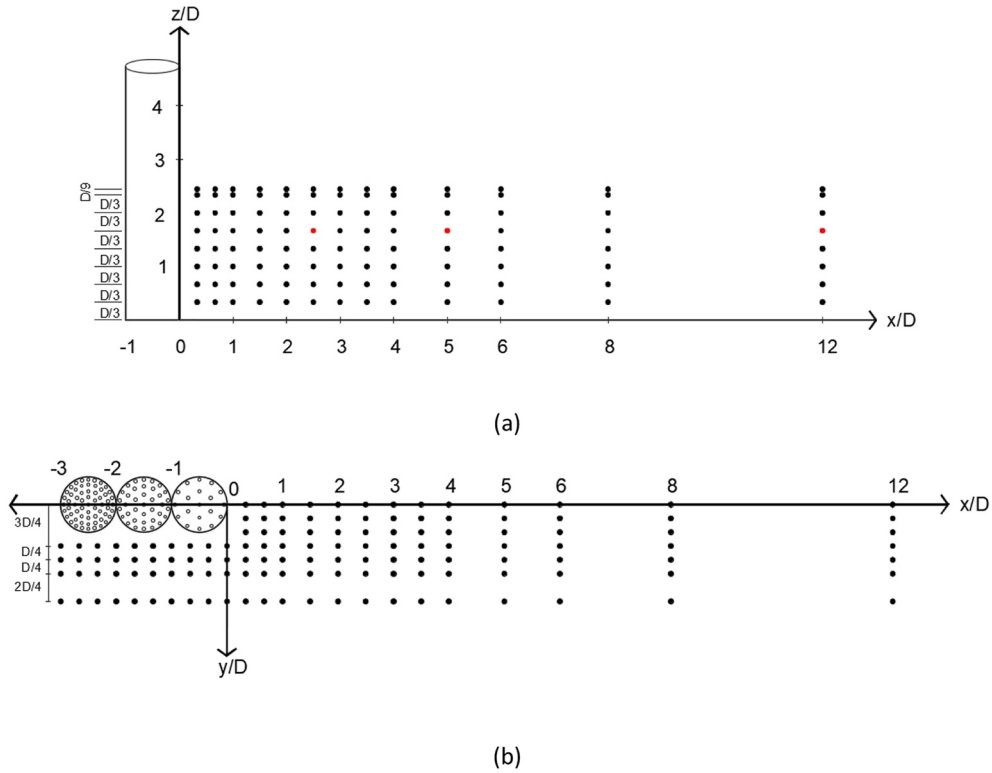

Figure 4. Measurements grid at the (a) vertical plane along the patch centerline and (b) horizontal plane in the middle of the water depth. Red dots indicate the locations of the points, where Joint Frequency Distribution (JFD) analysis was performed.

do not always secure that there will be no outliers in the data (Mori et al., 2007). Thus, the obtained data were despiked with the phase-space thresholding method of Goring and Nikora (2002) as amended by Wahl (2003). The outliers were replaced with cubic polynomial interpolation. The incoming depth-averaged mean velocity, U_0, was equal to 0.29 m/s for all experiments. U_0 was measured sufficiently upstream from the obstacles to be considered undisturbed and at a location where the flow was fully developed.

In addition to velocity measurements, flow visualization experiments were also conducted. The major idea behind these experiments was to gain a better insight into the role of patch expansion (i.e., development of midstream vegetation) on pairs of vortices observed in the wake region. To attain this aim, flow visualization experiments were conducted for the three characteristics cases with patch expansion (Figure 3). A traverser system, which has a 1.85 m distance to the water surface, was constructed onto the flume frame, to mount the camera on it. In this manner, the flow visualization records can be taken with a wide-angle. Food dye with a specific weight of 10.06 kN/m^3 was utilized during the tests. The dye was released in a synchronized manner from two separate openings with 5 mm diameter. Two openings were placed just between the center of the patch and the side-edges. Two different colors were employed to observe the mixing of the pairs of vortices from both sides in the wake region clearly.

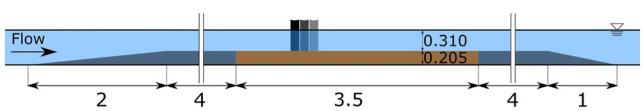

Figure 5. Description of the false bed that was constructed in the flume for the scour experiments. The brown area indicates the sand-pit, while the black, dark gray, and light gray cylinders indicate the dense, medium, and sparse vegetation patch, respectively. All dimensions are in meter.

2.4. Scour Experiments and Laser-Scanning of the Bed

The scour experiments were conducted by installing a false bed with metal sheets on top of the flume bed (Figure 5). The total length of the false bed was 14.5 m and covered the whole flume width. The height of the false bed was 0.205 m with a gentle slope (≈1V/5H) transitioning the flow from the flume bed elevation to the false bed elevation. A sand pit with 3.5 m length was placed into the middle of the false bed, which was filled up to the false bed height with coarse sand having a median diameter of $d_{50} = 0.52$ mm and a standard geometric deviation of $\sigma_g = \sqrt{d_{84}/d_{16}} = 1.85$. Before each scour

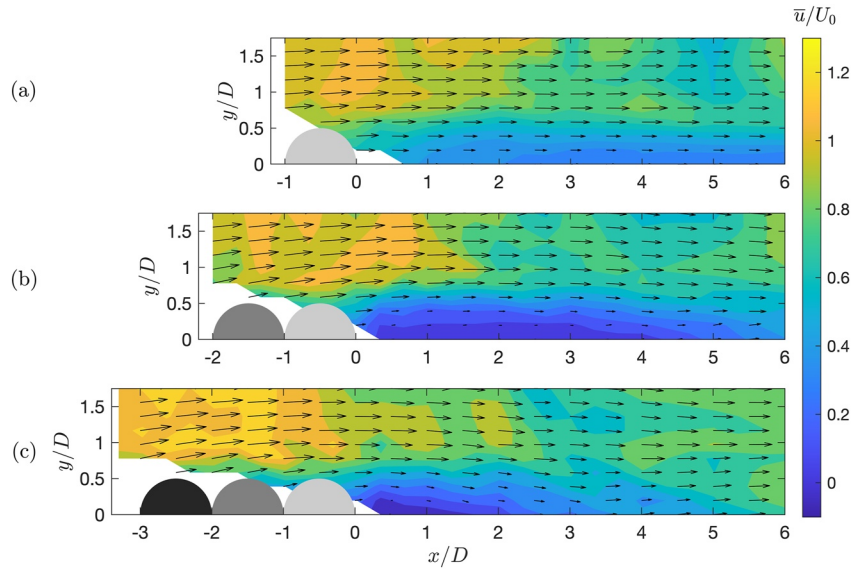

Figure 6. Contour plots of the normalized mean streamwise velocity, $\overline{u}/U_0$, for (a) an isolated sparse patch, (b) a composite patch that consists of a medium and a sparse patch at the upstream and downstream side, respectively, and (c) a composite patch that consists of a dense, a medium, and a sparse patch, from the upstream to the downstream side, respectively. The flow is from left to right.

experiment, the sand-bed in the pit was carefully leveled, and the flume was gradually filled with water until the desired water depth was reached. Subsequently, the pumps were turned on, the flow was maintained steady for precisely 8 hours without interruption. After 8 hours, the pumps were turned off and the flume was slowly drained without disturbing the scour pattern. The same approach and configuration for scour experiments was also used by Kitsikoudis et al. (2017) and Yagci et al. (2017).

A Leica ScanStation C10 laser scanner was utilized to obtain the 3D point cloud of the scoured bed. This device has the capability of measuring the coordinates of all the points in the region of interest in the horizontal and vertical directions. The sediment pit was scanned by this pulse-based laser-scanner before and after each experiment from approximately 1 m distance. The scanning process was conducted from six different locations around the pit to provide data integrity and high-resolution 3D point clouds. Data integrity was achieved, by registering the 3D point clouds from each of these six different stations, and as such, a merged high-resolution 3D point cloud with no data gaps was obtained. All the scanning tests were realized in medium resolution, which implies the instrument scans the surface with 1 mm grid from 1 m distance. Further details about the flume, sediment characteristics, sediment pit, and laser scanner measurement can be found in Kitsikoudis et al. (2017). Based on laser scanner measurements, the morphometric characteristics of scour patterns were acquired. These morphometrics characteristics were, maximum observed scour depth, width, and volume of local scour hole; local scour area in planview; deposition area (global deposition); maximum deposition height; upstream and downstream slope belonging to scour hole. Furthermore, the form factor, which is equal to scour volume divided by the cube of scouring width (Yagci et al., 2016), was also used in morphometric assessments. This parameter quantifies the locality of the scoured volume efficiently.

3. Analysis of the Experimental Results

3.1. Flow Kinematics

The isolated sparse patch exhibits a long steady-wake region with low velocity (Figures 6 and 7) and suppressed turbulent kinetic energy (TKE) (Figure 8) in agreement with previous studies (e.g., Chen et al., 2012). The elongation of the vegetation patch is accompanied by an increase in the upstream patch density (Section 3.2), the combination of which modifies significantly the near-patch flow field and shortens the steady-wake region (Figures 6 and 7). When the upstream part of the elongated patch becomes denser (i.e., stage 2), it diverts laterally a larger portion of the flow (Figure 6), with the rest of the flow penetrating the patch as bleed flow, leading to the development of a lateral shear layer with a steeper velocity gradient. As a result, the turbulent mixing downstream

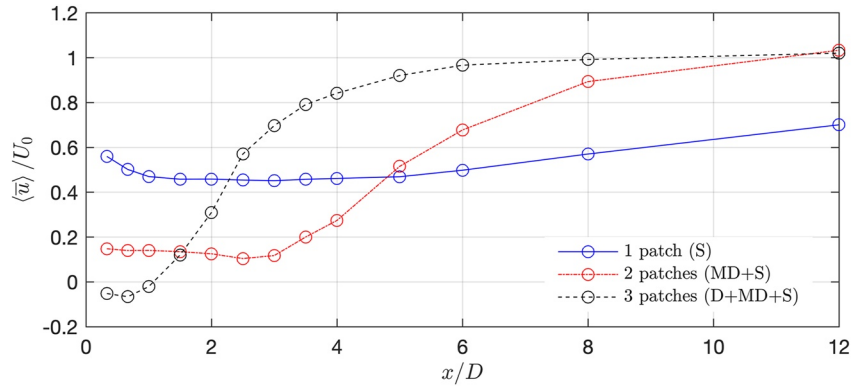

Figure 7. Longitudinal profiles of normalized mean flow velocity, $\overline{u}/U_0$, along the patch centerline at $z/D = 1.8$ for vegetation patches at different idealized growing stages.

of the patch due to lateral momentum transfer becomes more intense (Figure 9) and accelerates the flow recovery process. As the upstream part of the vegetation patch becomes denser (i.e., stage 3), the flow structure resembles the classical picture of the flow around a rigid pile (Sumer & Fredsøe, 2002, p. 151). The mean streamwise velocity in the wake of the isolated sparse patch does not start to considerably increase before a distance of 6*D* from the downstream edge of the patch, while as the vegetation patch expands and becomes denser, the mean streamwise velocity starts to increase after 3*D* and 1*D* downstream of the patch edge for the medium-sparse and dense-medium-sparse case, respectively (Figure 7).

It is worth mentioning that both the lateral turbulence intensity (Figure 9) and TKE (Figure 8) at the immediate downstream of the single sparse patch (stage 1) are reduced when the medium sparse patch is placed (representing the development stage) although turbulence intensity at further downstream (4–5*D*) is remarkably increased. Furthermore, the formation of a distinct steady-wake region in the case of stage 1 also contributes to the hindering of the turbulence at the immediate downstream of the patch.

The point at which the streamwise flow velocity begins to increase along the centerline in the wake of the patch (Figure 7) is the point at which the two lateral shear layers begin to interact. In isolated circular patches of sufficient density, this interaction forms a von Karman vortex street with a steep increase of velocity and TKE (Zong & Nepf, 2012). Despite composite patches of vegetation having spatially complex shape and density, there is a well-defined oscillatory pattern in transverse flow velocities of the development and mature stages of the patches (Figure 9). This can be regarded as the clear manifestation of von Karman vortex street due to vortex shedding. This characteristic oscillatory pattern in these two cases is also represented by a distinct peak in the power spectral densities of the transverse velocities (Figure 10). The slope of the power spectral densities follows the −5/3 law in the inertial subrange before becoming affected by the noise floor of the ADV at the higher sampling frequencies. It should be noted that even in the case of single sparse patch,

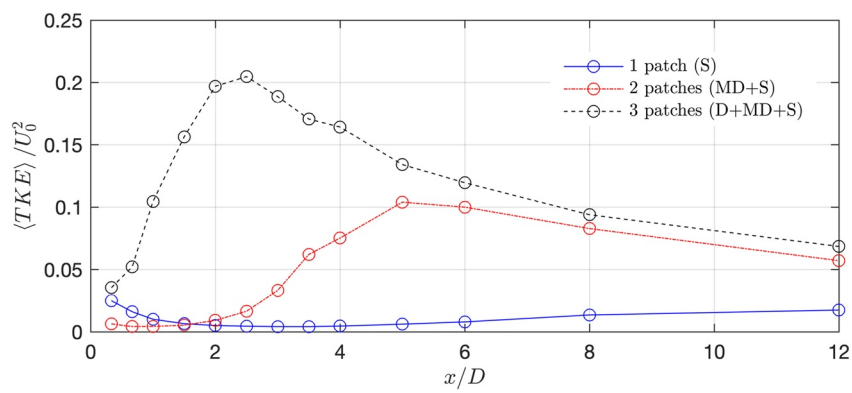

Figure 8. Longitudinal profiles of normalized TKE, k/U_0^2, along the patch centerline at $z/D = 1.8$ for vegetation patches at different idealized growing stages.

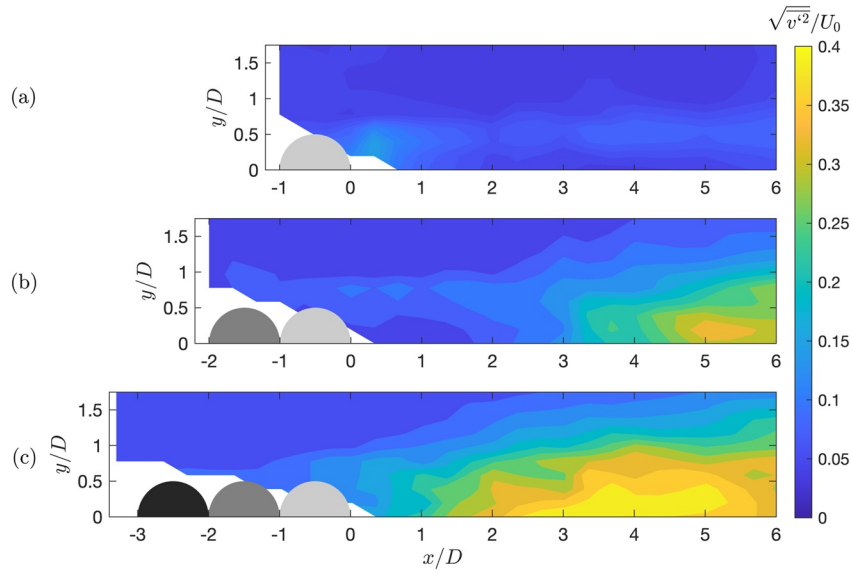

Figure 9. Contour plots of the normalized transverse turbulence intensity, $\sqrt{v'^2}/U_0$, for (a) an isolated sparse patch, (b) a composite patch that consists of a medium and a sparse patch at the upstream and downstream side, respectively, and (c) a composite patch that consists of a dense, a medium, and a sparse patch, from the upstream to the downstream side, respectively. The flow is from left to right.

poorly periodic oscillations matching with the vortex-shedding frequency of the patch are seen at $12D$ downstream which is not presented here for reasons of space. Still, the increasing trend of TKE toward downstream in the wake of the single sparse patch can be seen from Figure 8. This observation indicates that, although very weakly established, a long steady-wake region can be formed at the downstream of even such a sparse patch of vegetation.

The turbulence pattern downstream of the vegetation patches can be also analyzed by means of joint frequency distributions (JFDs), as previously done by Kitsikoudis et al. (2016, 2017), which shows the joint probabilities of the turbulent fluctuations of two different velocity components. Figure 11 shows the joint frequency distributions of the instantaneous longitudinal and transverse velocities normalized by the respective turbulence intensities for the three examined stages given in Figure 3. The JFDs were presented at three different distances from the downstream edge of the examined three stages. The von Karman vortex street downstream of stage 2 and downstream of stage 3 exhibited a bimodal distribution of the instantaneous transverse velocities. The detected two modes have symmetric character around the horizontal axis, that is, the instantaneous streamwise velocities (Figure 11). In the third stage, the proximity of bimodal distribution to the patch gets closer to the patch compared to the second stage. This is essentially due to the fact that when density increases, the point where the von Karman vortex street begins to form moves closer to the patch. The wake of the isolated sparse patch does not present a clear von Karman vortex street, as can be inferred by the lack of a distinct peak in the power spectral densities (Figure 10) and the weakly-correlated relationship between the instantaneous streamwise and transverse velocities (Figure 11).

Figure 12 presents the streamwise velocity profiles along the centerline of the flume for the three investigated stages. As seen from Figure 12, the velocity profile is much less affected by the presence of the patch in the single patch case of stage 1 compared to the other cases due to the stronger bleed flow. For the cases of stages 2 and 3, it is clearly seen that in the wake region the near-bed flow recovers earlier compared to the main body of the flow, due to the bed-generated turbulence. More specifically, bed generated turbulence near the bed pushes the boundary layer separation point around the patch toward downstream, and accelerates the recovery process. The implication of the formation of a von Karman vortex street near the downstream edge of the denser vegetation patch is that the deposition zone of the incoming suspended sediment downstream of the patch will become shorter due to the earlier increase in the turbulence (i.e., enhanced lateral mixing) within the wake.

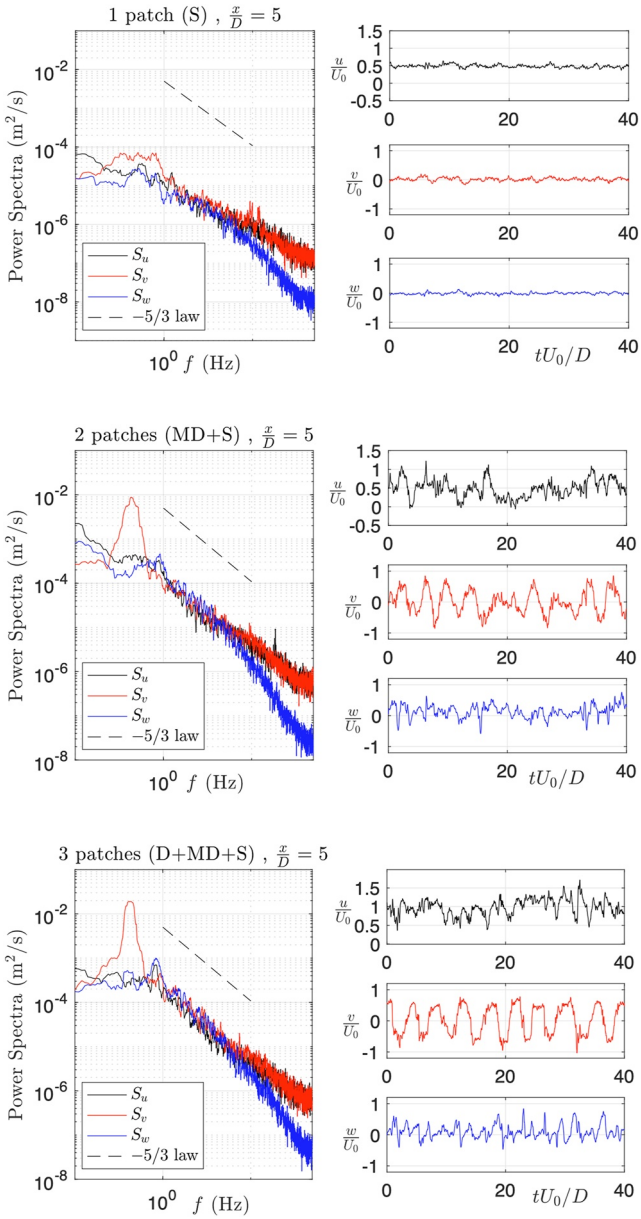

Figure 10. Power spectral densities of normalized flow velocities for (a) an isolated sparse patch, (b) a composite patch that consists of a medium and a sparse patch at the upstream and downstream side, respectively, and (c) a composite patch that consists of a dense, a medium, and a sparse patch, from the upstream to the downstream side, respectively.

3.2. Flow Visualization

Flow visualization records obtained for the three characteristic cases of the patch, which simulate three different stages of the streamlined vegetation patch, are presented in Figure 13. The photos given in Figure 13 were obtained from Movies S1, S2, and S3 which are the records taken during flow visualization tests conducted for three characteristic patch cases. The phenomenon of separation around a body is essentially a consequence of the combined impact of geometry induced adverse pressure gradient, as well as the retardance of the flow in the boundary layer (Afzalimehr et al., 2016; Schlichting, 1968, p. 121). The scale of the eddies generated in the wake region is greatly controlled by the velocity deficit between the wake region and the contraction zone. Hence, the patterns of vortices observed in the wake regions of the three characteristic patch cases can be sought as the clear manifestation of strength of the shear layer (Sumer & Fredsøe, 2002, 2006). It should be also noted that when flow passes through/around a permeable body, the presence of bleed flow lessens the strength of shear layer, and brings about a delay in the formation of von Karman vortex street in the wake region (Chen et al., 2012; Zong & Nepf, 2012). Thus, the dye released from both sides of the patch moves for a while in the streamwise direction without lateral mixing as observed from Figure 13a.

Based on this background, it is evident from Figure 13 that the length of the steady-wake region decreases with the additional patches and finally is minimized in stage 3 (Figure 13c). Two shear layers, which are not converged yet are observed in stage 1, whereas in stage 3 (Figure 13c) a von-Karman vortex street is highly distinct and there is a clear convergence point where the von Karman vortices start, about 1-2D downstream of the patch, which seems to agree with Figures 5–7. With the expansion of the patch from stage 1-to-stage 3, both the SVF of the patch and the length of the vegetated zone increases.

Because it has a greater potential to build a more developed boundary layer, any elongated obstacle has a more streamlined form than a non-elongated obstacle with the same projection area. While the elongation of the obstruction is likely to delay lateral mixing, increased SVF is expected to cause earlier lateral mixing. The experiments revealed that, of these two factors (elongation and patch densification, both of which have opposing impacts on vorticities), densification prevails over patch expansion/elongation.

These findings can be interpreted such that the patch expansion process alters not only the length of the steady-wake region but also the scale of the pairs of vortices generated at both sides of the body. It is known that the generated vortices typically scale with the dimension of the cylinder. Due to the kinematic reasons discussed above (i.e., decreased bleed flow and increased contraction effect owing to the plant growth), the patch tends to respond to the flow like a solid cylinder as a consequence of the patch's expansion. Consequently, both the size and the frequency of the vortices increase. While the sparse case does not generate a secondary flow pattern that would indicate an intensive vorticity, in the dense case vorticity is pronounced and vortex induced lateral mixing emerges immediately after the obstacle. While due to pronounced bleed flow passage through the obstacle no circular pairs of vortices were monitored for the sparse case, for the dense case they are obvious. In the next sub-section, further discussion on the effect of flow alteration on scour/deposition processes is presented.

3.3. Morphometric Analysis of the Scour Pattern

Observed scoured bed patterns present key clues about the secondary flow structures, which are generated as a consequence of the interaction between flow and vegetation. These patterns reflect the ability of the flow

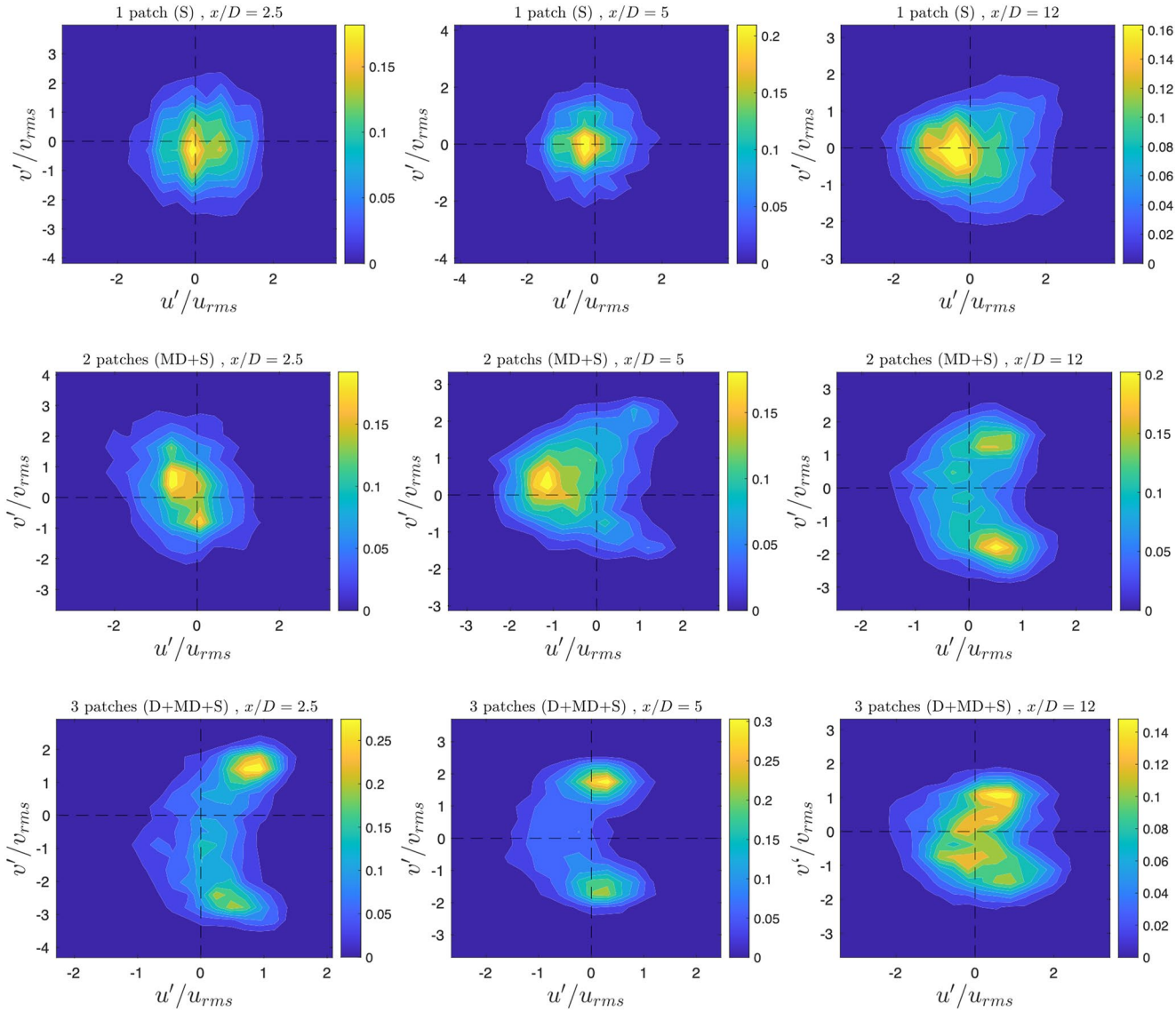

Figure 11. Joint frequency distributions (JFD) of instantaneous longitudinal velocities normalized with the longitudinal turbulence intensity, $u'/\sqrt{\overline{u'^2}}$, and instantaneous transverse velocities normalized with the transverse turbulence intensity, $v'/\sqrt{\overline{v'^2}}$. The location of the JFDs are x/D = 2.5, 5, and 12, respectively. These points were denoted in measurement grid as red dots in Figure 2.

in terms of transporting/depositing the sediment at different locations. The surface plots of the scour patterns examined for 5 different cases of vegetation patch are presented in Figure 14. Based on the scans given in Figure 14, the morphometric characteristics of the scoured/deposited patterns were obtained, and they are presented in Table 3.

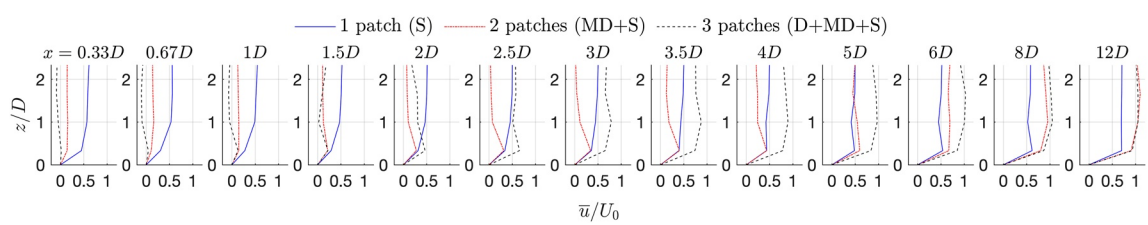

Figure 12. Profiles of the normalized mean streamwise velocities along the patch centerline. The location of each profile is indicated at the top of each subfigure.

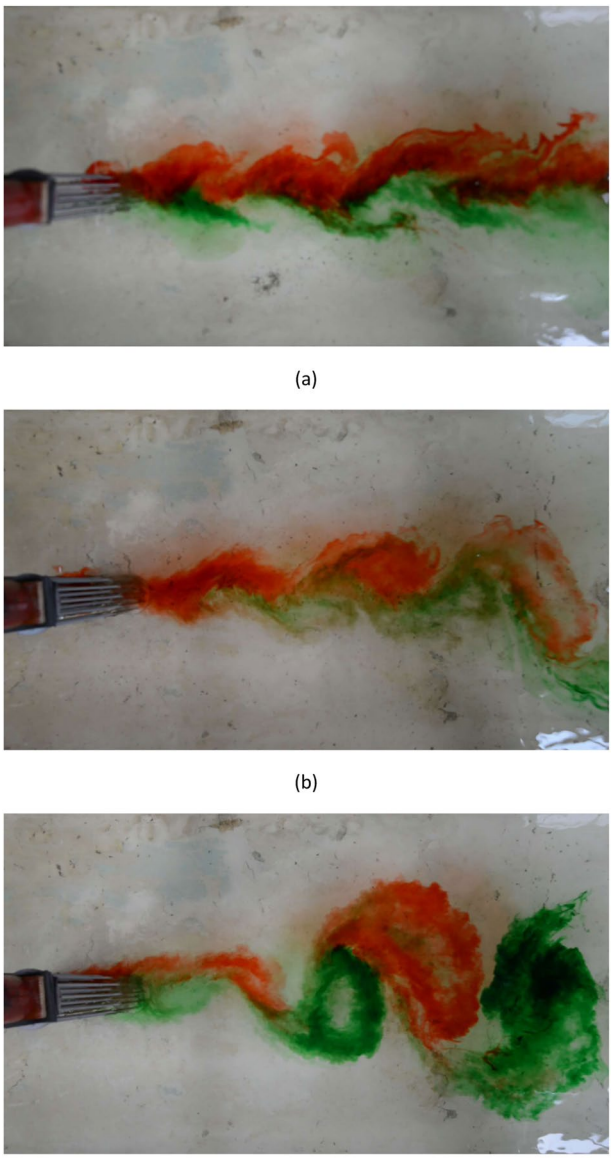

Figure 13. Instantaneous views belonging to: (a) Stage 1, (b) Stage 1 and (c) Stage 3 from flow visualization experiments. The videos in which this figure is extracted from are presented as Supporting Information S1.

The scour patterns presented in Figure 14 demonstrate that with the expansion of the representative vegetative patch (i.e., decreased permeability and increased blockage volume), the width and depth of the scour increase. In line with this situation, the deposition height and volume around the patch increase as well. According to Kitsikoudis et al. (2016), for a typical isolated permeable obstacle, the strength of downflow, which is the major contributor of prominent coherent structures near the bottom, increases with the decrease in permeability and increase in blockage (i.e., or SVF). Likewise, the increment in scour observed for representative patch expansion in Figure 14 can be explained by the fact that the strength of the downflow increases due to the patch expansion-induced decrease in permeability. Consequently, as a clear manifestation of the increased strength of separation at the upstream base of the body (Majd et al., 2016) and the horseshoe vortex (Graf & Istiarto, 2002; Unger & Hager, 2007), the observed scour depth and width increases.

Another result that can be drawn from Figure 14 is that, without exception, all the permeable patch cases generate a sharp-crested elongated ridge in the streamwise direction. A recent study by Aksel et al. (2021) showed that with the development of the scour hole around a solid cylinder, lee-wake vortices, which control the wake region in the rigid bottom case, evolves to large-scale counter-rotating streamwise vortices (LSCSVs). Despite this study was performed for a solid cylinder, the presence of LSCSVs shown by Aksel et al. (2021) seems reasonable to explain the ridge in Figure 14. Thus, the sharp-crested ridge can be considered as the footprint of this scour-induced secondary flow pattern. However, further studies are needed to clarify this process.

In addition to the qualitative assessments given in the previous paragraph, a quantitative-based analysis is presented in Figure 15 to gain a better insight into the impact of patch expansion on the bed processes. The cross-sections of scoured bed taken from the centerlines of the consecutive permeable vegetation models are given in Figures 15a and 15b, respectively, for stages 2 and 3. Comparative analysis of these cross-sections reveals that while the scour depth decreases in the streamwise direction within the scour hole, the side slopes of the scour hole, which scale with the angle of repose of the bed sediment, remain unchanged.

In Figure 15c, the scour cross-sections of isolated patches are given, whereas Figure 15d presents the scour cross-sections of the three stages taken from the upstream patch. As can be seen from Figure 15c, the vegetation patches with different SVF produce very similar (almost identical) forms in terms of morphometric ratios (e.g., width-to-depth ratio or slope of the scour hole). Direct comparison between the scour cross-sections of isolated patch cases (Figure 15c) and the upstream patch in growth stages (Figure 15d) shows that the process of representative patch expansion renders the morphometry of scour holes different from the case of the isolated patches. The patch expansion process does not affect only the morphometrical ratios belonging to the local scour. It dramatically amplifies the global scour as well.

The process of patch expansion and its direct consequences on flow pattern and river bed morphology demonstrate itself not only in the wake region but also in the contraction zone. As explained in Section 3.1, the stages of representative patch expansion or the cases of increase in density of isolated patch cause a remarkable augmentation in lateral momentum flux between the wake and the contraction region. This situation leads to a shortening in the steady-wake region. Furthermore, another significant impact of the representative expansion process on the flow field is that the contraction effect becomes more prominent as the patch expands (Figure 6). As a result of this process, significant increase in erosion in the contraction zone, that is, amplified global scour, was detected (Figures 15a–15c). This effect becomes even more pronounced for stage 3 given in Figure 15a.

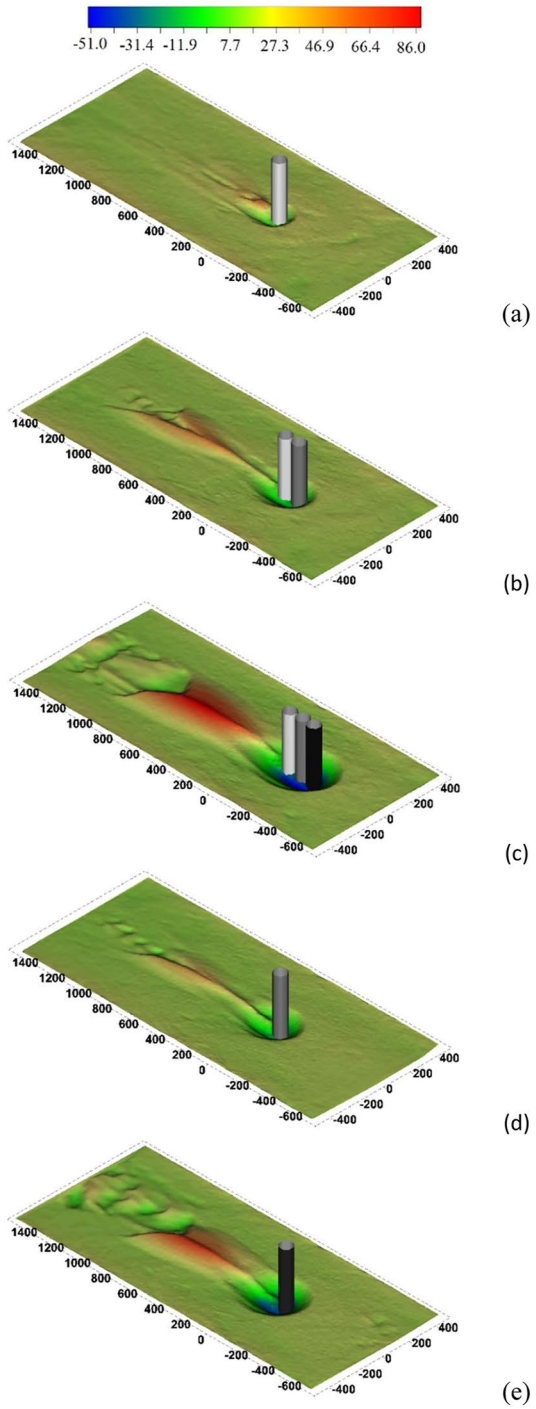

Figure 14. The scour patterns observed around (a) initial (b) development (c) mature stages of patch expansion process. The isolated (d) medium, (e) dense obstacles are given as reference cases. White, gray and black cylinders represent the sparse, medium and dense arrays of cylinders. All the units are in mm and flow direction is from right-to-left.

In Figure 16, the longitudinal scour profiles along the flume centerline belonging to the examined cases are presented. Ripple developments are observed at the end of the deposited mound in all the cases, but the case of stage 1. The ripples tend to scale with the size of the deposited mound behind which they emerge, that is, the greater the mound, the larger the size of the ripples. Also, it is seen that differing from the side slopes of the scour hole, the downstream slopes of the holes exhibit different character from each other. This is the manifestation that the downstream part of the scour hole is sensitive to existing coherent flow structures, which are directly controlled by the imposed patch configuration. Also, the study by Yagci et al. (2016) revealed that with the decreasing porosity of the patch, the distance between the deposition region and the obstacle becomes shorter as a consequence of decreased steady-wake region. All the cases tested but single-sparse patch case confirm this assertion.

In Figure 17, the morphometric scour characteristics are plotted to make a quantitative analysis. It is evident from Figure 17 that the expansion process of the patch enhances the scour depth, width, and volume both in local and global scale. During the representative patch expansion, the projection area against the flow, which is regarded as a primary hydrodynamic factor according to the drag-force equation, remains unchanged. Despite this fact, the difference between scour characteristics belonging to the cases of stage 2–3, and the corresponding isolated reference cases is considerably distinct. As discussed above, increase of drag due to patch expansion strengthens the coherent structures near the bottom. In line with this fact, both Figures 14 and 16 show that during the growing process of the patch, with the effect of the decreasing porosity, the deposition zone becomes localized and scour hole gains a more elongated form. The variation of form factors, P_f, with respect to patch configurations are given in Figure 16d. The variation of form factors also verify that the localization of scour hole increases during the representative patch expansion.

4. Discussion, Recommendations, and Limitations

Establishment and self-organization processes of patchy vegetation are controlled by the flow pattern (temporal flow variability in discharges), sediment regime (size, quantity, sorting, and distribution of transported sediment), basin conditions (e.g., density of vegetation on the hill slopes, soil properties, basin morphometry), biological, and chemical factors. The development of the river vegetation is governed overwhelmingly by flow and sediment regimes rather than other secondary factors mentioned above (Baattrup et al., 2006; Riis & Biggs, 2003). Nilsson and Svedmark (2002) assert that the development and spatial distribution of plants in active channels are predominantly influenced by the prevailing flow and sediment regimes, whereas biological and chemical variables assume a subordinate role in this intricate phenomenon. In view of this fact, the present study focused only on the physical interactions between instream vegetation, flow and sediment. The less influential components of the process (i.e., biological and chemical variables) were ignored.

The aim of this research was to examine the effect of patch enlargement on flow kinematics and morphological processes in its proximity. It is important to note that throughout the scour experiments, each step of the patch growth process was addressed independently. There was no realistic temporal transition between stages 1 and 2 or between stages 2 and 3. Instead, each step was individually reproduced in flume experiments by modifying the patch design (intensifying the

Table 3
Summary of Morphometric Characteristics Belonging to Scour and Deposition[a]

Exp No	Experiment	S_d (cm)	S_w (cm)	S_v (cm^3)	S_a (cm^2)	D_a (cm^2)	D_h (cm)	U-S (%)	D-S (%)
1	Isolated sparse: Stage 1	2.8	22.7	563	399	486	2.5	−52	+38
2	Sparse + Medium: Stage 2	5.2	29.0	1,696	855	2,144	2.6	−55	+12
3	Sparse + Medium + Dense: Stage 3	8.6	41.8	5,783	1,614	2,773	5.1	−64	+22
4	Isolated dense	7.6	37.9	3,409	1,130	1,881	3.9	−60	+20
5	Isolated medium	5.5	30.7	1,331	807	942	1.9	−59	+22

[a]S_d is the maximum observed scour depth, S_w is the scour width of local scour hole, S_v is the scour volume of local scour hole, S_a is the local scour area in plan view, D_a is the deposition area (global deposition), D_h is the maximum observed deposition height, U-S is the upstream slope, D-S is the downstream slope.

density and elongating the patch). After setting up each independent patch configuration in the flume, identical initial conditions (horizontal intact bed condition and steady discharge) were applied to the vegetative obstruction in order to examine the effect of actual patch features on the scour pattern. The obtained findings should be interpreted from this perspective.

In this study, we have conducted experiments, aiming at improving our understanding of the hydrodynamic outcomes of patch expansion process. Combined impact of two basic physical processes were accounted for in patch expansion, namely lengthening of patch and increasing stem density. As aforementioned, these two mutually excluding hydrodynamic factors may have different weights on flow kinematics around the patch for different instream species. The primary research questions were centered around the influence of these mutually excluding two hydrodynamic factors. Furthermore, the experiments presented here were conducted under idealized conditions.

Aquatic, and intertidal species (e.g., *Salix*, *Populus*, *Alnus* and *Spartina Anglica*) in which the flow structure around them previously examined by Vandenbruwaene et al. (2011) and Cornacchia et al. (2022), usually have a complex distribution of the volume in vertical. This specie-specific volume distribution adds further complication to the flow structure (Kitsikoudis et al., 2016; Wilson, Yagci, Rauch, & Steosser, 2006). In spite of this fact, the utilization of the rigid stem analogy, which has been employed in numerous prior investigations (Chang & Constantinescu, 2015; Chang et al., 2017; Yamasaki et al., 2019; Zong and Nepf, 2012), was chosen as the approach for this study in order to maintain simplicity in addressing the problem. However, in reality, depending on their moisture retention ability, plants display different flexibility against drag force. While this flexibility is even more pronounced for the vegetation in perennial streams, the instream plants observed in ephemeral streams have relatively higher flexural rigidity due to lower moisture availability. The flexibility induced bending in trunk (Kitsikoudis et al., 2017; Majd et al., 2016) and streamlining/reconfiguration at a leaf scale (Albayrak et al., 2012) of vegetative obstructions intensely affects the coherent flow structures, drag force (Fathi-Maghadam & Kouwen, 1997; Wilson, Yagci, Rauch, & Olsen, 2006), scour around the vegetation (Yagci et al., 2016) at the individual-scale, and hydraulic resistance (Carollo et al., 2005; Freeman et al., 2000; Wu et al., 1999) at the reach scale. During the experimental study, these factors (i.e., bending, streamlining, complex volumetric distribution of plant) were ignored to identify the influence of the patch expansion process on kinematic characteristics and scouring more directly. In other words, these factors were excluded considering it would not be rational to tackle all the relevant questions within a single study. After gaining a comprehensive understanding of the idealized scenario (i.e., the rigid stem analogy), it is plausible to systematically incorporate additional variables into experimental or numerical cases in future research. Future research is expected to include the examination of specific species, the influence of plants' intricate volumetric organization on flow and morphological processes, and the effects of bending, streamlining, foliage, and water depth. It is possible to identify the underlying correlation between each factor and the observed outcomes using a systematic and sequential approach.

While hydrodynamics plays a key role on the patch size and density through propagule deposition, other factors such as oxygen and nutrient availability affect the survival and growth of seedlings within the vegetation patch. As a result, there is an expected upper limit of the patch density, which cannot be exceeded, thus securing the existence of a steady-wake flow region and favorable flow conditions for the continuous extension of the patch. Indeed, such long vegetation patches in nature were detected and presented by Larsen and Harvey (2011). The solid volume fraction values of the tested patches vary within the range of 0.188 and 0.059

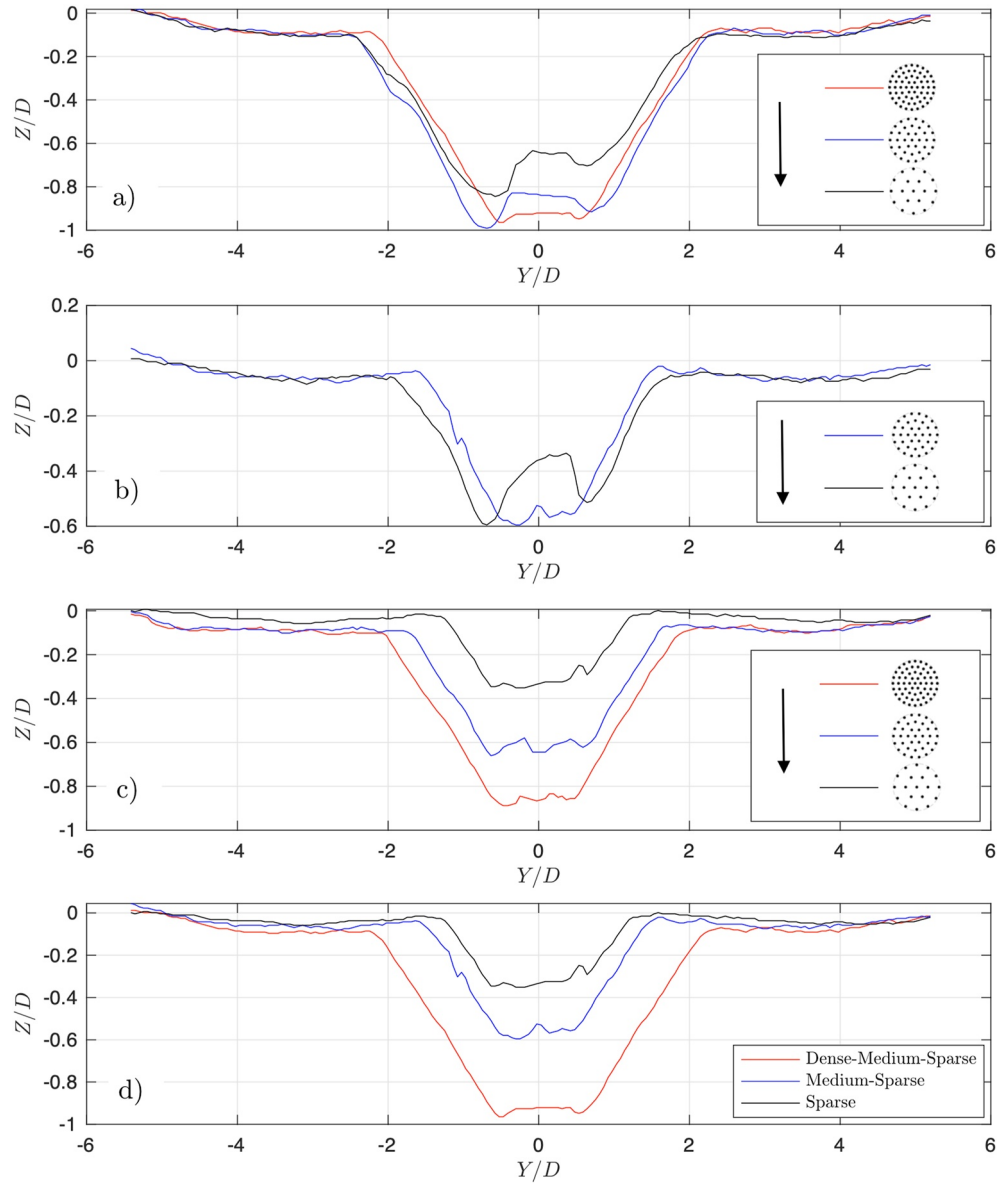

Figure 15. The scoured cross-sections located (a–b) at the centerline of the consecutive permeable vegetation patches for mature and developing stages respectively (the legends shows the actual location of the cross-section), (c) at the centerline of the isolated patches (the legends shows the actual location of the cross-section for isolated patches), (d) at the centerline of the upstream patches belonging to initial, developing and mature stages. The ordinate values are given based on the local coordinate values created by the laser scanner measurement during the measurement. The center of the obstacle is $Y/D = 0$.

in this study. Yagci and Kabdasli (2008) measured the SVF of *Pinus Pinea*, *Thuja Orientalis*, and *Cupressus Macrocarpa* and found that SVF values of these species were 0.005, 0.004, and 0.005 for 0.25 m water depth. In their study, Wilson, Yagci, Rauch, and Steosser (2006) checked the variation of volume with respect to height of an individual *Salix fragilis*, which is commonly observed in river corridors. As can be seen from Figure 4 given in Wilson, Yagci, Rauch, and Steosser (2006), for the height of 0.301 m (i.e., the water depth in our experiments) of the plant, the volume corresponds to approximately 0.08–0.1 dm^3. In this study, the submerged volumes of the plants were 0.112, 0.218, and 0.360 L for the height of 0.301 m. Viewed this way, it can be stated that the SVF of the patches in this study were slightly higher compared to actual plants. On the other hand, SVF values in present study are in harmony with the SVFs values (0.1–0.04) tested in the study of Zong and Nepf (2012) and the values (0.028–0.51) examined by Chen et al. (2012). From the hydrodynamic perspective, the patch with higher density causes weaker bleed flow, shorter steady wake region, stronger

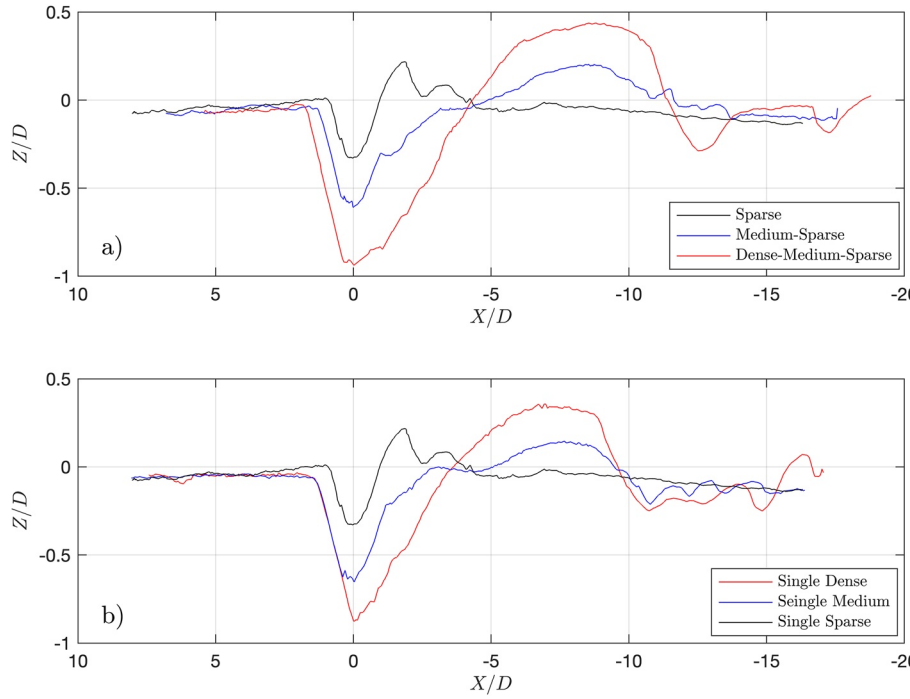

Figure 16. Longitudinal scour profiles along the flume centerline (a) for growing stages of patches (i.e., initial stage: sparse, development stage: medium-sparse, mature stage: dense-medium-sparse), and (b) isolated patches. The direction of the flow is from left to right (→). The center of the obstacle is $X/D = 0$.

lateral shear layer, and more distinct pairs of vortices (Yagci et al., 2021a) in the wake region compared to natural patches with lower SVF. The benefit of this situation is that the flow recovery region becomes shorter due to intensive lateral momentum transfer. As this is not a scaled laboratory study, and the main objective is to understand how patch expansion affects bed morphology and the flow field, the chosen SVFs serve well to achieve this objective.

In natural rivers, the spatial distribution of vegetation exhibits different characteristics for ephemeral and perennial rivers. The mosaic of the species emerges as superimposed impacts of the basin geology, climate, flow regime, sedimentary process, biological and chemical factors inside the river corridor. The weights of these components that control the distribution of vegetation communities along the river corridors are basin-specific. However, among these, the flow and sediment regimes have always had a particular significance in terms of governing the development of river plants. The propagules, which are transported under the effect of flow, are deposited on the river bed during the recession stages of high flows (Danvind & Nilsson, 1997; Ward et al., 1999). Later on, these propagules buried into the incoming sediment mixtures develop and initiate the formation of pioneer-islands as described in detail in Introduction section. These pioneer islands are highly influential in terms of capturing sediment (Ashworth et al., 2000; Schoelynck et al., 2012), stabilizing the fluvial regime (Bertoldi et al., 2014) producing well-functioning deeper and narrower cross-sections (Ikeda & Izumi, 1990; Millar & Quick, 1993; Montgomery, 2011; Valyrakis et al., 2021), and improving habitat diversity (Gurnell & Petts, 2002). Within this perspective, in this study, the continuous growth process of the instream vegetation patch, which arises as an output of complex reciprocal interaction between plant-flow-sediment in a river, was discretized and represented with three consecutive stages in an idealized manner. These discretized patch expansion stages were exposed to flow in flume experiments.

In the scour experiments, uniform-like bed material was used differing from natural river beds, which means that the armoring effect is ignored. It is also known that for the experiments conducted under clear water conditions, which is the case in the present study, the equilibrium depth of scouring may be overly conservative (Melville & Chiew, 1999). Besides, throughout the tests, the Reynolds number was kept constant. It should be noted that different kinematic characteristics and scour patterns can be obtained under different Reynolds numbers. Therefore, the obtained results should be interpreted within this vision.

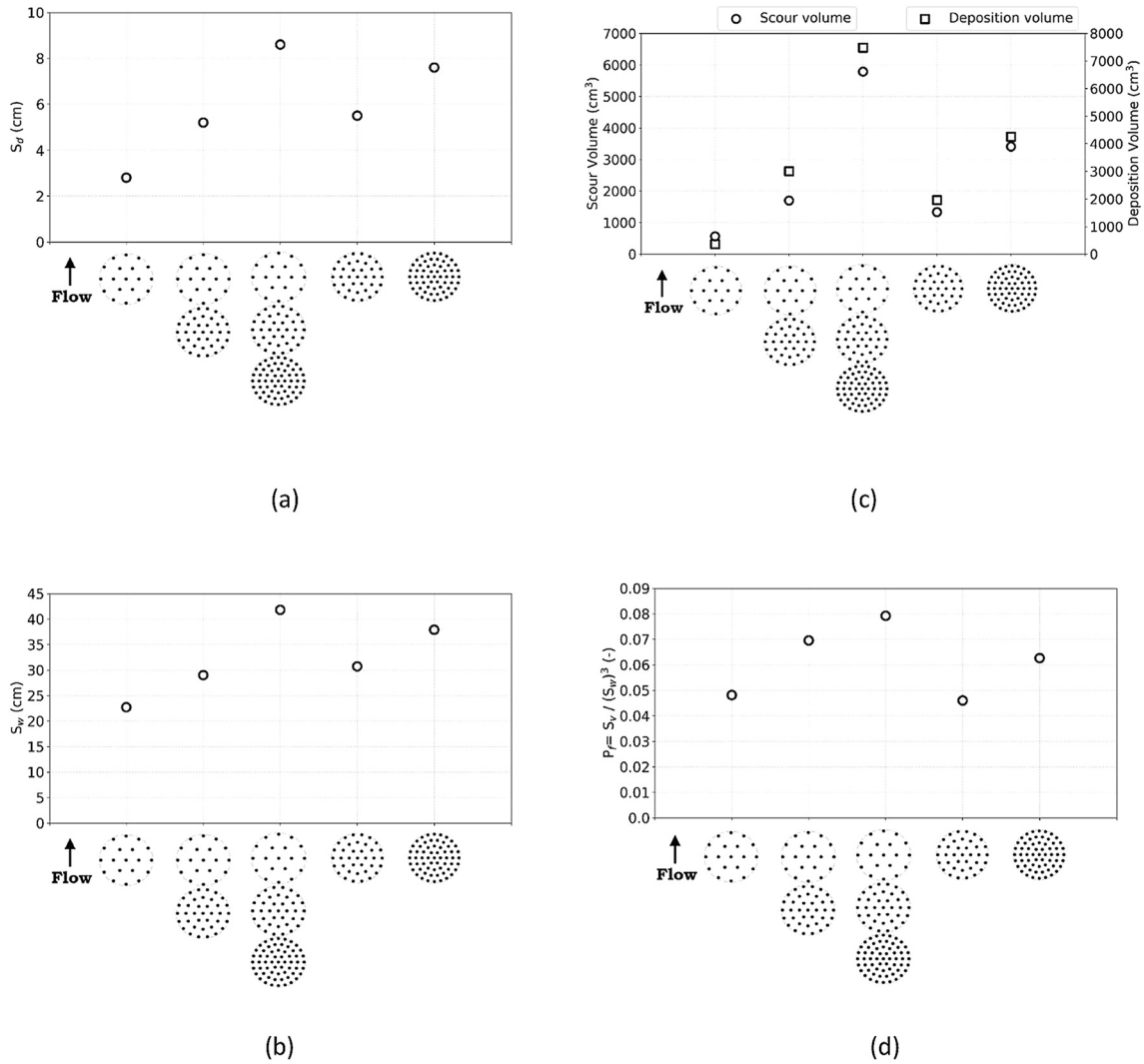

Figure 17. The variation of (a) scour depth (S_d), (b) local scour width (S_w), (c) local scour volume (S_v), and (d) fom factor (P_f) with respect to different patch configurations.

In light of the arguments presented above, for future studies, it is recommended to investigate the role of bending, streamlining, and complex volumetric distribution of plants on flow and scour characteristics. Despite the inclusion of these factors may make the analysis of the problem more difficult, it can greatly aid in building knowledge that is essential for developing sustainable river management strategies. While doing this, it should be noted that these temporally varying plant features display different characteristics during the growth process.

5. Conclusions

In this study, three growth stages of an instream vegetation patch, with respect to the longitudinal (streamwise) expansion of the patch, were simulated independently from each other by means of idealized/simplified porous cylinders with different porosities. Velocity and turbulence measurements as well as flow visualization tests were conducted in rigid-bed experiments, which were followed by scour experiments conducted on loose bed conditions. In addition to the three stages of the elongated vegetation patch, reference scour tests with single medium and dense patches were also conducted. The following major conclusions were drawn from this study.

According to the measurements, the spatial growth of deposition behind the isolated sparse vegetation patch is prone to be elongated in the early phases (e.g., stages 1–2). This is because a prominent steady wake zone induces a weak lateral velocity profile (i.e., a weak lateral shear layer), which delays the onset of large-scale von Karman

vortex street. This condition leads suspended sediment to deposit in an elongated form rear the patch. The experiments also demonstrated that as the patch lengthened and the density increased, scour volume and height of the mound increased. In this case, the deposited mound emerges more locally due to the mitigated bleed flow and enhanced lateral mixing (i.e., early formation of von-Karman vortex street). Therefore, for the dense and long form of the patch, early recovery of flow in the wake zone inhibits deposition at a longer distance (i.e., stage 3) and ultimately limits the spread of the deposited mound in the wake zone. This aids in explaining why vegetative patches in streams have restricted longitudinal growth.

The streamlined extension of the vegetative obstacle is a key hydrodynamic element that plays a critical role in deposition processes. It was also seen that the scouring geometry is dictated not just by the densest portion of the patch, but also by the entire patch. Although streamlined elongation is a hydrodynamically favorable form for impermeable materials (e.g., extended bridge piers), it has been witnessed that this kind of vegetative blockage dramatically magnifies global scour. In addition, streamlined elongated patch increases the localization (i.e., the hole becomes deeper and narrower) of the local scour.

Measurements of velocity revealed that the patch expansion alters not only the coherent flow patterns in plan view, but also the vertical velocity distribution in the wake zone. The vertical velocity profile in the wake dramatically deviates from the logarithmic profile as the patch expands and becomes denser. Compared to the upper part of the flow, the velocity profile close to the bed region recovers relatively sooner. This rapid recovery of velocity close to the bed can be explained by the increased turbulence detected close to the bottom as a result of the influence of enhanced contraction.

Lastly, laser scanner measurements revealed that the ripples developed behind the deposited mound tend to scale with the size of the mound, which is regulated considerably by the patch's physical characteristics and the strength of the lateral momentum transfer.

Data Availability Statement

The presented data in this study was obtained in the Hydraulics Laboratory of Istanbul Technical University. The data set is available in Yagci et al. (2021b).

Acknowledgments
This study was conducted under the support of the Scientific Research Funding Program of ITU-BAP, Project Number: 39544. The authors would like to thank the technicians Mr. H. Yalcin, Mr. M. Ulucinar, and Mr. Y. Aktaş in Hydraulics Laboratory of Istanbul Technical University for their effort and sincere friendship during the experiments.

References

Afzalimehr, H., Moradian, M., Gallichand, J., & Sui, J. (2016). Effect of adverse pressure gradient and different vegetated banks on flow. *River Research and Applications*, *32*(5), 1059–1070. https://doi.org/10.1002/RRA.2908

Aksel, M., Yagci, O., Kirca, V. S. O., Erdog, E., & Heidari, N. (2021). A comparative analysis of coherent structures around a pile over rigid-bed and scoured-bottom. *Ocean Engineering*, *226*, 108759. https://doi.org/10.1016/J.OCEANENG.2021.108759

Albayrak, I., Nikora, V., Miler, O., & O'hare, M. (2012). Flow-plant interactions at a leaf scale: Effects of leaf shape, serration, roughness and flexural rigidity. *Aquatic Sciences*, *74*(2), 267–286. https://doi.org/10.1007/s00027-011-0220-9

Ashworth, P. J., Best, J. L., Roden, J. E., Bristow, C. S., & Klaassen, G. J. (2000). Morphological evolution and dynamics of a large, sand braidbar, Jamuna River, Bangladesh. *Sedimentology*, *47*(3), 533–555. https://doi.org/10.1046/J.1365-3091.2000.00305.X

Baattrup-Pedersen, A., Szoszkiewicz, K., Nijboer, R., O'Hare, M., & Ferreira, T. (2006). Macrophyte communities in unimpacted European streams: Variability in assemblage patterns, abundance and diversity. *The Ecological Status of European Rivers: Evaluation and Intercalibration of Assessment Methods*, 179–196. https://doi.org/10.1007/978-1-4020-5493-8_13

Bal, K., Struyf, E., Vereecken, H., Viaene, P., De Doncker, L., de Deckere, E., et al. (2011). How do macrophyte distribution patterns affect hydraulic resistances? *Ecological Engineering*, *37*(3), 529–533. https://doi.org/10.1016/j.ecoleng.2010.12.018

Bardossy, A., & Caspary, J. (1990). Theoretical and applied climatology detection of climate change in Europe by analyzing European atmospheric circulation patterns from 1881 to 1989. *Theoretical and Applied Climatology*, *42*(3), 155–167. https://doi.org/10.1007/bf00866871

Bayazit, M., (2001). *Hydrology* (pp. 230). Birsen Publishing Company.

Bertoldi, W., Siviglia, A., Tettamanti, S., Toffolon, M., Vetsch, D., & Francalanci, S. (2014). Modeling vegetation controls on fluvial morphological trajectories. *Geophysical Research Letters*, *41*(20), 7167–7175. https://doi.org/10.1002/2014GL061666

Bouma, T. J., Friedrichs, M., Van Wesenbeeck, B. K., Temmerman, S., Graf, G., & Herman, P. M. J. (2009). Density-dependent linkage of scale-dependent feedbacks: A flume study on the intertidal macrophyte Spartina anglica. *Oikos*, *118*(2), 260–268. https://doi.org/10.1111/J.1600-0706.2008.16892.X

Camporeale, C., Perucca, E., Ridolfi, L., & Gurnell, A. M. (2013). Modeling the interactions between river morphodynamics and riparian vegetation. *Reviews of Geophysics*, *51*(3), 379–414. https://doi.org/10.1002/ROG.20014

Carollo, F. G., Ferro, V., & Termini, D. (2005). Flow resistance law in channels with flexible submerged vegetation. *Journal of Hydraulic Engineering*, *131*(7), 554–564. https://doi.org/10.1061/(ASCE)0733-9429(2005)131:7(554)

Chang, K., & Constantinescu, G. (2015). Numerical investigation of flow and turbulence structure through and around a circular array of rigid cylinders. *Journal of Fluid Mechanics*, *776*, 161–199. https://doi.org/10.1017/JFM.2015.321

Chang, W.-Y., Constantinescu, G., & Tsai, W. F. (2017). On the flow and coherent structures generated by a circular array of rigid emerged cylinders placed in an open channel with flat and deformed bed. *Journal of Fluid Mechanics*, *831*, 1–40. https://doi.org/10.1017/JFM.2017.558

Chen, Z., Ortiz, A., Zong, L., & Nepf, H. (2012). The wake structure behind a porous obstruction and its implications for deposition near a finite patch of emergent vegetation. *Water Resources Research*, *48*(9), 9517. https://doi.org/10.1029/2012WR012224

Chow, V. T. (1959). *Open-channel hydraulics* (p. 680). McGraw-Hill.
Cornacchia, L., Riviere, N., Doppler, D., Vallier, F., & Puijalon, S. (2022). Flow and wake length downstream of live submerged vegetation patches: How do different species and patch configurations create sheltering in stressful habitats? *Water Resources Research*, *58*(3), 1–21. https://doi.org/10.1029/2021WR030880
Danvind, M., & Nilsson, C. (1997). Seed floating ability and distribution of alpine plants along a northern Swedish river. *Journal of Vegetation Science*, *8*(2), 271–276. https://doi.org/10.2307/3237356
Fathi-Maghadam, M., & Kouwen, N. (1997). Nonrigid, nonsubmerged, vegetative roughness on floodplains. *Journal of Hydraulic Engineering*, *123*(1), 51–57. https://doi.org/10.1061/(ASCE)0733-9429(1997)123:1(51)
Follett, E. M., & Nepf, H. M. (2012). Sediment patterns near a model patch of reedy emergent vegetation. *Geomorphology*, *179*, 141–151. https://doi.org/10.1016/J.GEOMORPH.2012.08.006
Freeman, G. E., Rahmeyer, W. H., & Copeland, R. R. (2000). Determination of resistance due to shrubs and woody vegetation. *Environmental Sciences*. https://doi.org/10.21236/ADA383997
Goring, D. G., & Nikora, V. I. (2002). Despiking acoustic Doppler velocimeter data. *Journal of Hydraulic Engineering*, *128*(1), 117–126. https://doi.org/10.1061/(ASCE)0733-9429(2002)128:1(117)
Graf, W. H., & Istiarto, I. (2002). Flow pattern in the scour hole around a cylinder. *Journal of Hydraulic Research*, *40*(1), 13–20. https://doi.org/10.1080/00221680209499869
Gurnell, A. (2014). Plants as river system engineers. *Earth Surface Processes and Landforms*, *39*(1), 4–25. https://doi.org/10.1002/ESP.3397
Gurnell, A., Bertoldi, W., & Corenblit, D. (2012). Changing river channels: The roles of hydrological processes, plants and pioneer fluvial landforms in humid temperate, mixed load, gravel bed rivers. *Earth-Science Reviews*, *111*(1–2), 129–141. https://doi.org/10.1016/J.EARSCIREV.2011.11.005
Gurnell, A. M., & Petts, G. E. (2002). Island-dominated landscapes of large floodplain rivers, a European perspective. *Freshwater Biology*, *47*(4), 581–600. https://doi.org/10.1046/J.1365-2427.2002.00923.X
Heidari, N., Yagci, O., & Aksel, M. (2021). Midchannel islands in lowland river corridors and their impacts on flow structure and morphology:A numerical based conceptual analysis. *Ecological Engineering*, *173*, 106419. https://doi.org/10.1016/J.ECOLENG.2021.106419
Heidelman, M., & Vural, D. C. (2023). Geomorphodynamics, evolution, and ecology of vertical roots. *Frontiers in Plant Science*, *14*. https://doi.org/10.3389/fpls.2023.1102491
Holzenthal, E. R., Wengrove, M. E., & Hill, D. F. (2022). Mechanisms of sediment transport around finite patches of submerged aquatic vegetation, Estuarine. *Coastal and Shelf Science*, *273*, 107905. https://doi.org/10.1016/j.ecss.2022.107905
Huai, W., Li, S., Katul, G. G., Liu, M., & Yang, Z. (2021). Flow dynamics and sediment transport in vegetated rivers: A review. *Journal of Hydrodynamics*, *33*(3), 400–420. https://doi.org/10.1007/s42241-021-0043-7
Ikeda, S., & Izumi, N. (1990). Width and depth of self-formed straight gravel rivers with bank vegetation. *Water Resources Research*, *26*(10), 2353–2364. https://doi.org/10.1029/WR026I010P02353
Jones, J. I., Collins, A. L., Naden, P. S., & Sear, D. A. (2012). The relationship between fine sediment and macrophytes in rivers. *River Research and Applications*, *28*(7), 1006–1018. https://doi.org/10.1002/RRA.1486
Kingora, K., & Sadat, H. (2022). Flow and scalar transfer characteristics for a circular colony of vegetation. *Physics of Fluids*, *34*(8), 083606. https://doi.org/10.1063/5.0090272
Kitsikoudis, V., Kirca, V. S. O., Yagci, O., & Celik, M. F. (2017). Clear-water scour and flow field alteration around an inclined pile. *Coastal Engineering*, *129*, 59–73. https://doi.org/10.1016/J.COASTALENG.2017.09.001
Kitsikoudis, V., Yagci, O., & Kirca, V. S. O. (2020). Experimental analysis of flow and turbulence in the wake of neighboring emergent vegetation patches with different densities. *Environmental Fluid Mechanics*, *20*(6), 1417–1439. https://doi.org/10.1007/S10652-020-09746-6
Kitsikoudis, V., Yagci, O., Kirca, V. S. O., & Kellecioglu, D. (2016). Experimental investigation of channel flow through idealized isolated tree-like vegetation. *Environmental Fluid Mechanics*, *16*(6), 1283–1308. https://doi.org/10.1007/S10652-016-9487-7
Klein, M. (1984). Anti clockwise hysteresis in suspended sediment concentration during individual storms: Holbeck Catchment; Yorkshire, England. *Catena*, *11*(2–3), 251–257. https://doi.org/10.1016/0341-8162(84)90014-6
Kohendal-Gargari, M., Kirca, V. S. O., & Yagci, O. (2021). Experimental investigation of gradually-varied unsteady flow passed a circular pile. *Coastal Engineering*. https://doi.org/10.1016/j.coastaleng.2021.103926
Kuhnle, R. A. (1992). Bed load transport during rising and falling stages on two small streams. *Earth Surface Processes and Landforms*, *17*(2), 191–197. https://doi.org/10.1002/ESP.3290170206
Larsen, L. G. (2019). Multiscale flow-vegetation-sediment feedbacks in low-gradient landscapes. *Geomorphology*, *334*, 165–193. https://doi.org/10.1016/J.GEOMORPH.2019.03.009
Larsen, L. G., & Harvey, J. W. (2011). Modeling of hydroecological feedbacks predicts distinct classes of landscape pattern, process, and restoration potential in shallow aquatic ecosystems. *Geomorphology*, *126*(3–4), 279–296. https://doi.org/10.1016/J.GEOMORPH.2010.03.015
Lima, P. H. S. D., Janzen, J. G., & Nepf, H. M. (2015). Flow patterns around two neighboring patches of emergent vegetation and possible implications for deposition and vegetation growth. *Environmental Fluid Mechanics*, *15*(4), 881–898. https://doi.org/10.1007/s10652-015-9395-2
Liu, M., Huai, W., & Ji, B. (2021). Characteristics of the flow structures through and around a submerged canopy patch. *Physics of Fluids*, *33*(3), 035144. https://doi.org/10.1063/5.0041782
Luhar, M., & Nepf, H. M. (2013). From the blade scale to the reach scale: A characterization of aquatic vegetative drag. *Advances in Water Resources*, *51*, 305–316. https://doi.org/10.1016/J.ADVWATRES.2012.02.002
Majd, S. F., Yagci, O., Kirca, V. S. O., & Kitsikoudis, V. (2016). Flow and turbulence around an inclined pile. In *Annual international ocean and polar engineering conference* (pp. 1087–1093). ISOPE.
Melville, B. W., & Chiew, Y.-M. (1999). Time scale for local scour at bridge piers. *Journal of Hydraulic Engineering*, *125*(1), 59–65. https://doi.org/10.1061/(ASCE)0733-9429(1999)125:1(59)
Millar, R. G., & Quick, M. C. (1993). Effect of bank stability on geometry of gravel rivers. *Journal of Hydraulic Engineering*, *119*(12), 1343–1363. https://doi.org/10.1061/(ASCE)0733-9429(1993)119:12(1343)
Montgomery, D. R. (2011). Geomorphology, river ecology, and ecosystem management. *Geomorphology, River Ecology, and Ecosystem Management*, 247–253. https://doi.org/10.1029/WS004P0247
Mori, N., Suzuki, T., & Kakuno, S. (2007). Noise of acoustic Doppler velocimeter data in bubbly flows. *Journal of Engineering Mechanics*, *133*(1), 122–125. https://doi.org/10.1061/(ASCE)0733-9399(2007)133:1(122)
Nilsson, C., & Svedmark, M. (2002). Basic principles and ecological consequences of changing water regimes: Riparian plant communities. *Environmental Management*, *30*(4), 468–480. https://doi.org/10.1007/S00267-002-2735-2
Ortiz, A. C., Ashton, A., & Nepf, H. (2013). Mean and turbulent velocity fields near rigid and flexible plants and the implications for deposition. *Journal of Geophysical Research: Earth Surface*, *118*(4), 2585–2599. https://doi.org/10.1002/2013JF002858

Palmer, M. A., Bernhardt, E. S., Allan, J. D., Lake, P. S., Alexander, G., Brooks, S., et al. (2005). Standards for ecologically successful river restoration. *Journal of Applied Ecology*, *42*(2), 208–217. https://doi.org/10.1111/J.1365-2664.2005.01004.X

Reid, I., Frostick, L. E., & Layman, J. T. (1985). The incidence and nature of bedload transport during flood flows in coarse-grained alluvial channels. *Earth Surface Processes and Landforms*, *10*(1), 33–44. https://doi.org/10.1002/ESP.3290100107

Riis, T., & Biggs, B. J. F. (2003). Hydrologic and hydraulic control of macrophyte establishment and performance in streams. *Limnology & Oceanography*, *48*(4), 1488–1497. https://doi.org/10.4319/LO.2003.48.4.1488

Sand-Jensen, K., & Pedersen, M. L. (2008). Streamlining of plant patches in streams. *Freshwater Biology*, *53*(4), 714–726. https://doi.org/10.1111/J.1365-2427.2007.01928.X

Schlichting, H. (1968). *Boundary-layer theory* (6th ed.). McGraw-Hill.

Schnauder, I., & Moggridge, H. L. (2009). Vegetation and hydraulic-morphological interactions at the individual plant, patch and channel scale. *Aquatic Sciences*, *71*(3), 318–330. https://doi.org/10.1007/S00027-009-9202-6

Schoelynck, J., De Groote, T., Bal, K., Vandenbruwaene, W., Meire, P., Temmerman, S., et al. (2012). Self-organised patchiness and scale-dependent bio-geomorphic feedbacks in aquatic river vegetation. *Ecography*, *35*(8), 760–768. https://doi.org/10.1111/J.1600-0587.2011.07177.X

Schwarz, C., Gourgue, O., Van Belzen, J., Zhu, Z., Bouma, T. J., Van De Koppel, J., et al. (2018). Self-organization of a biogeomorphic landscape controlled by plant life-history traits. *Nature Geoscience*, *11*(9), 672–677. https://doi.org/10.1038/s41561-018-0180-y

Silva, R., Rodrigues, S., & Vieira, A. (2023). Role of vegetation inducing sedimentation in an artificial earth channel. *Mercator*, *22*(1), 1–21. https://doi.org/10.4215/rm2023.e22003

Solari, L., Van Oorschot, M., Belletti, B., Hendriks, D., Rinaldi, M., & Vargas-Luna, A. (2016). Advances on modelling riparian vegetation—Hydromorphology interactions. *River Research and Applications*, *32*(2), 164–178. https://doi.org/10.1002/RRA.2910

Song, T., & Graf, W. H. (1996). Velocity and turbulence distribution in unsteady open channel flows. *Journal of Hydraulic Engineering*, *122*(3), 141–154. https://doi.org/10.1061/(ASCE)0733-9429(1996)122:3(141)

Stein, A., Gerstner, K., & Kreft, H. (2014). Environmental heterogeneity as a universal driver of species richness across taxa, biomes and spatial scales. https://doi.org/10.1111/ele.12277

Stride, B., Abolfathi, S., Odara, M. G. N., Bending, G. D., & Pearson, J. (2023). Modeling microplastic and solute transport in vegetated flows. *Water Resources Research*, *59*(5), e2023WR034653. https://doi.org/10.1029/2023WR034653

Sumer, B. M., & Fredsøe, J. (2002). *The mechanics of scour in the marine environment*. World Scientific.

Sumer, M., & Fredsøe, J. (2006). Hydrodynamics around cylindrical structures (revised edition) (pp. 1–530). https://doi.org/10.1142/6248/SUPPL_FILE/6248_CHAP01.PDF

Temmerman, S., Bouma, T. J., Van de Koppel, J., Van der Wal, D., De Vries, M. B., & Herman, P. M. J. (2007). Vegetation causes channel erosion in a tidal landscape. *Geology*, *35*(7), 631–634. https://doi.org/10.1130/G23502A.1

Thomas, R. E., Schindfessel, L., McLelland, S. J., Creëlle, S., & De Mulder, T. (2017). Bias in mean velocities and noise in variances and covariances measured using a multistatic acoustic profiler: The Nortek Vectrino profiler. *Measurement Science and Technology*, *28*(7), 075302. https://doi.org/10.1088/1361-6501/AA7273

Turker, U., Yagci, O., & Kabdasli, M. S. (2019). Impact of nearshore vegetation on coastal dune erosion: Assessment through laboratory experiments. *Environmental Earth Sciences*, *78*(19), 584. https://doi.org/10.1007/s12665-019-8602-8

Unger, J., & Hager, W. H. (2007). Down-flow and horseshoe vortex characteristics of sediment embedded bridge piers. *Experiments in Fluids*, *42*, 1–19. https://doi.org/10.1007/s00348-006-0209-7

Valyrakis, M., Liu, D., Turker, U., & Yagci, O. (2021). The role of increasing riverbank vegetation density on flow dynamics across an asymmetrical channel. *Environmental Fluid Mechanics*, *21*(3), 643–666. https://doi.org/10.1007/s10652-021-09791-9

Vandenbruwaene, W., Temmerman, S., Bouma, T. J., Klaassen, P. C., de Vries, M. B., Callaghan, D. P., et al. (2011). Flow interaction with dynamic vegetation patches: Implications for biogeomorphic evolution of a tidal landscape. *Journal of Geophysical Research*, *116*(F1), F01008. https://doi.org/10.1029/2010JF001788

Vreugdenhil, S. J., Kramer, K., & Pelsma, T. (2006). Effects of flooding duration, -frequency and -depth on the presence of saplings of six woody species in north-west Europe. *Forest Ecology and Management*, *236*(1), 47–55. https://doi.org/10.1016/J.FORECO.2006.08.329

Wahl, T. L. (2003). Discussion of "Despiking acoustic Doppler velocimeter data" by Derek G. Goring and Vladimir I. Nikora. *Journal of Hydraulic Engineering*, *129*(6), 484–487. https://doi.org/10.1061/(asce)0733-9429(2003)129:6(484)

Wang, X., Huai, W., & Cao, Z. (2021). An improved formula for incipient sediment motion in vegetated open channel flows. *International Journal of Sediment Research*, *37*(1), 47–53. https://doi.org/10.1016/J.IJSRC.2021.06.001

Ward, J. V., Tockner, K., Arscott, D. B., & Claret, C. (2002). Riverine landscape diversity. *Freshwater Biology*, *47*(4), 517–539. https://doi.org/10.1046/J.1365-2427.2002.00893.X

Ward, J. V., Tockner, K., Edwards, P. J., Kollmann, J., Bretschko, G., Gurnell, A. M., et al. (1999). A reference river system for the Alps: The fiume tagliamento. *Regulated Rivers: Research & Management*, *15*(1–3), 63–75. https://doi.org/10.1002/(SICI)1099-1646(199901/06)15:1/3

Wharton, G., Cotton, J. A., Wotton, R. S., Bass, J. A. B., Heppell, C. M., Trimmer, M., et al. (2006). Macrophytes and suspension-feeding invertebrates modify flows and fine sediments in the Frome and Piddle catchments, Dorset (UK). *Journal of Hydrology*, *330*(1–2), 171–184. https://doi.org/10.1016/J.JHYDROL.2006.04.034

Wilson, C. A. M. E., Yagci, O., Rauch, H. P., & Olsen, N. R. B. (2006). 3D numerical modelling of a willow vegetated river/floodplain system. *Journal of Hydrology*, *327*(1–2), 13–21. https://doi.org/10.1016/J.JHYDROL.2005.11.027

Wilson, C. A. M. E., Yagci, O., Rauch, H.-P., & Stoesser, T. (2006). Application of the drag force approach to model the flow-interaction of natural vegetation. *International Journal of River Basin Management*, *4*(2), 137–146. https://doi.org/10.1080/15715124.2006.9635283

Wu, F.-C. W., Shen, H. W., & Chou, Y.-J. (1999). Variation of roughness coefficients for unsubmerged and submerged vegetation. *Journal of Hydraulic Engineering*, *125*(9), 934–942. https://doi.org/10.1061/(asce)0733-9429(1999)125:9(934)

Wu, H., Cheng, N. S., & Chiew, Y. M. (2021). Bed-load transport in vegetated flows: Phenomena, parametrization, and prediction. *Water Resources Research*, *57*(4), e2020WR028143. https://doi.org/10.1029/2020wr028143

Yagci, O., Celik, M. F., Kitsikoudis, V., Ozgur Kirca, V. S., Hodoglu, C., Valyrakis, M., et al. (2016). Scour patterns around isolated vegetation elements. *Advances in Water Resources*, *97*, 251–265. https://doi.org/10.1016/J.ADVWATRES.2016.10.002

Yagci, O., & Kabdasli, M. S. (2008). The impact of single natural vegetation elements on flow characteristics. *Hydrological Processes*, *22*(21), 4310–4321. https://doi.org/10.1002/HYP.7018

Yagci, O., Karabay, O., & Strom, K. (2021a). Bleed flow structure in the wake region of finite array of cylinders acting as an alternative supporting structure for foundation. *Journal of Ocean Engineering and Marine Energy*, *7*(4), 379–403. https://doi.org/10.1007/S40722-021-00208-9

Yagci, O., Ozgur Kirca, V. S., Wilson, C. A. M. E., Kitsikoudis, V., Celik, M. F., & Sertkan, C. (2021b). Data_Yagci_Water_Resources_Research_2021 [Dataset]. Hydroshare. http://www.hydroshare.org/resource/a502428b140348f4942c3d457457dea4

Yagci, O., & Strom, K. (2022). Reach-scale experiments on deposition process in vegetated channel: Suspended sediment capturing ability and backwater effect of instream plants. *Journal of Hydrology*, *608*, 127612. https://doi.org/10.1016/J.JHYDROL.2022.127612

Yagci, O., Yildirim, I., Celik, M. F., Kitsikoudis, V., Duran, Z., & Kirca, V. S. O. (2017). Clear water scour around a finite array of cylinders. *Applied Ocean Research*, *68*, 114–129. https://doi.org/10.1016/J.APOR.2017.08.014

Yager, E. M., & Schmeeckle, M. W. (2013). The influence of vegetation on turbulence and bed load transport. *Journal of Geophysical Research: Earth Surface*, *118*(3), 1585–1601. https://doi.org/10.1002/JGRF.20085

Yamasaki, T. N., de Lima, P. H. S., Silva, D. F., Preza, C. G. D. A., Janzen, J. G., & Nepf, H. M. (2019). From patch to channel scale: The evolution of emergent vegetation in a channel. *Advances in Water Resources*, *129*, 131–145. https://doi.org/10.1016/J.ADVWATRES.2019.05.009

Yuksel, A. Y. (2018). Flow structure at the downstream of a one-line riparian emergent tree along the floodplain edge in a compound open-channel flow. *Journal of Hydrodynamics*, *30*(3), 470–480. https://doi.org/10.1007/s42241-018-0052-3

Zong, L., & Nepf, H. (2012). Vortex development behind a finite porous obstruction in a channel. *Journal of Fluid Mechanics*, *691*, 368–391. https://doi.org/10.1017/jfm.2011.479